Title
NAAA-regulated lipid signaling governs the transition from acute to chronic pain

Journal
Science Advances, 7(43)

ISSN
2375-2548

Authors
Fotio, Yannick
Jung, Kwang-Mook
Palese, Francesca
et al.

Publication Date
2021-10-22

DOI
10.1126/sciadv.abi8834

NEUROSCIENCE

NAAA-regulated lipid signaling governs the transition from acute to chronic pain

Yannick Fotio[1], Kwang-Mook Jung[1], Francesca Palese[1], Andre Obenaus[2], Alex Mabou Tagne[1], Lin Lin[1], Tarif Ibne Rashid[1], Romario Pacheco[3†], Amandine Jullienne[2], Jade Ramirez[1], Marco Mor[4], Gilberto Spadoni[5], Cholsoon Jang[6], Andrea G. Hohmann[3], Daniele Piomelli[1]*

Chronic pain affects 1.5 billion people worldwide but remains woefully undertreated. Understanding the molecular events leading to its emergence is necessary to discover disease-modifying therapies. Here we show that N-acylethanolamine acid amidase (NAAA) is a critical control point in the progression to pain chronicity, which can be effectively targeted by small-molecule therapeutics that inhibit this enzyme. NAAA catalyzes the deactivating hydrolysis of palmitoylethanolamide, a lipid-derived agonist of the transcriptional regulator of cellular metabolism, peroxisome proliferator-activated receptor-α (PPAR-α). Our results show that disabling NAAA in spinal cord during a 72-h time window following peripheral tissue injury halts chronic pain development in male and female mice by triggering a PPAR-α-dependent reprogramming of local core metabolism from aerobic glycolysis, which is transiently enhanced after end-organ damage, to mitochondrial respiration. The results identify NAAA as a crucial control node in the transition to chronic pain and a molecular target for disease-modifying medicines.

INTRODUCTION

Acute pain after physical trauma can evolve, in vulnerable individuals, into a chronic pain state that long outlasts tissue healing and is often resistant to therapy (*1*, *2*). Nerve damage is considered a critical driving factor in this transition, but the molecular events underlying it are still poorly understood (*3*, *4*). Yet, delineating the nature, localization, and timing of such events is necessary to uncover control nodes in the pain chronification process, which could be targeted by disease-modifying medicines (*5*). Current research efforts are focused on synaptic (*3*) and immune (*4*, *6*) adaptations that occur, both peripherally and centrally, following end-organ damage, although deficits in neuronal energy balance are also receiving serious consideration (*7*, *8*).

The intracellular cysteine hydrolase *N*-acylethanolamine acid amidase (NAAA) (*9*, *10*) catalyzes the degradation of palmitoylethanolamide (PEA), an endogenous lipid agonist of the nuclear receptor peroxisome proliferator–activated receptor-α (PPAR-α) (*11*). This ligand-operated transcription factor serves important regulatory functions in both cellular metabolism and the defensive response to noxious stimuli (*12*). Consistent with this dual role, activation of PPAR-α by exogenous PEA attenuates pain (*11*, *13*) and inflammation (*14*) and stimulates mitochondrial respiration (*15*). These findings prompted us to ask whether NAAA-regulated PEA signaling at PPAR-α might contribute to the emergence of chronic pain after somatic injury, when the pressure to bring about adaptive neuroplastic changes intensifies the demand for bioenergy in peripheral and central nociceptive neurons (*3*, *16*). Our results show that end-organ damage produces a transient enhancement of NAAA expression and a consequent suppression of PEA-mediated signaling in innervating segments of the spinal cord. This event redirects local metabolism from high energy–yielding mitochondrial respiration toward biomass-generating aerobic glycolysis, a phenomenon akin to the Warburg effect first described in proliferating cancer cells (*17*). Disabling NAAA during this critical time window restores normal PEA-mediated PPAR-α activation, stops metabolic reprogramming, and aborts the transition to pain chronicity. This action identifies NAAA and its cognate signaling complex as a druggable molecular target for the prevention of chronic pain.

RESULTS

Chemical end-organ damage causes a chronic pain–like state in vulnerable mice

To investigate the role of NAAA in the transition to pain chronicity, we adapted the formalin model (*18*) to allow evaluation of both immediate responses to end-organ lesion and progression to a persistent pain–like state (*19*, *20*). The latter was characterized by assessing key signs of severe chronic pain in humans, including spontaneous pain; bilateral and extraterritorial spreading of sensitization (*21*, *22*); disturbances in emotional, cognitive, and vegetative function (*23*, *24*); and microstructural reorganization of forebrain circuits involved in the regulation of stress and emotion (*25*, *26*). We injected escalating doses of formalin (0.1, 0.3, or 1% volume, 20 μl) into the hind paw of male mice and monitored them for the subsequent 4 months. As expected from prior work (*18*), the irritant evoked an immediate nocifensive reaction that at the 1% dose lasted >60 min and was associated with robust local inflammation (fig. S1, A and B). The pain behavior elicited by 1% formalin, but not 0.1 or 0.3%, was followed in ~80% of the animals (67 of 84) by lasting bilateral hypersensitivity to mildly noxious heat stimuli and normally innocuous mechanical stimuli, which appeared within 24 to 48 hours

[1]Department of Anatomy and Neurobiology, University of California Irvine, Irvine, CA 92697, USA. [2]Department of Pediatrics, University of California Irvine, Irvine, CA 92697, USA. [3]Psychological and Brain Sciences, Program in Neuroscience, and Gill Center for Biomolecular Science, Indiana University, Bloomington, IN 47401, USA. [4]Dipartimento di Scienze degli Alimenti e del Farmaco, Università di Parma, 43124 Parma, Italy. [5]Dipartimento di Scienze Biomolecolari, Università di Urbino "Carlo Bo," 61029 Urbino, Italy. [6]Department of Biological Chemistry, University of California Irvine, Irvine, CA 92697, USA.
*Corresponding author. Email: piomelli@hs.uci.edu
†Present Address: Graduate Program in Neuroscience, University of Arizona, Tucson, AZ 85721, USA.

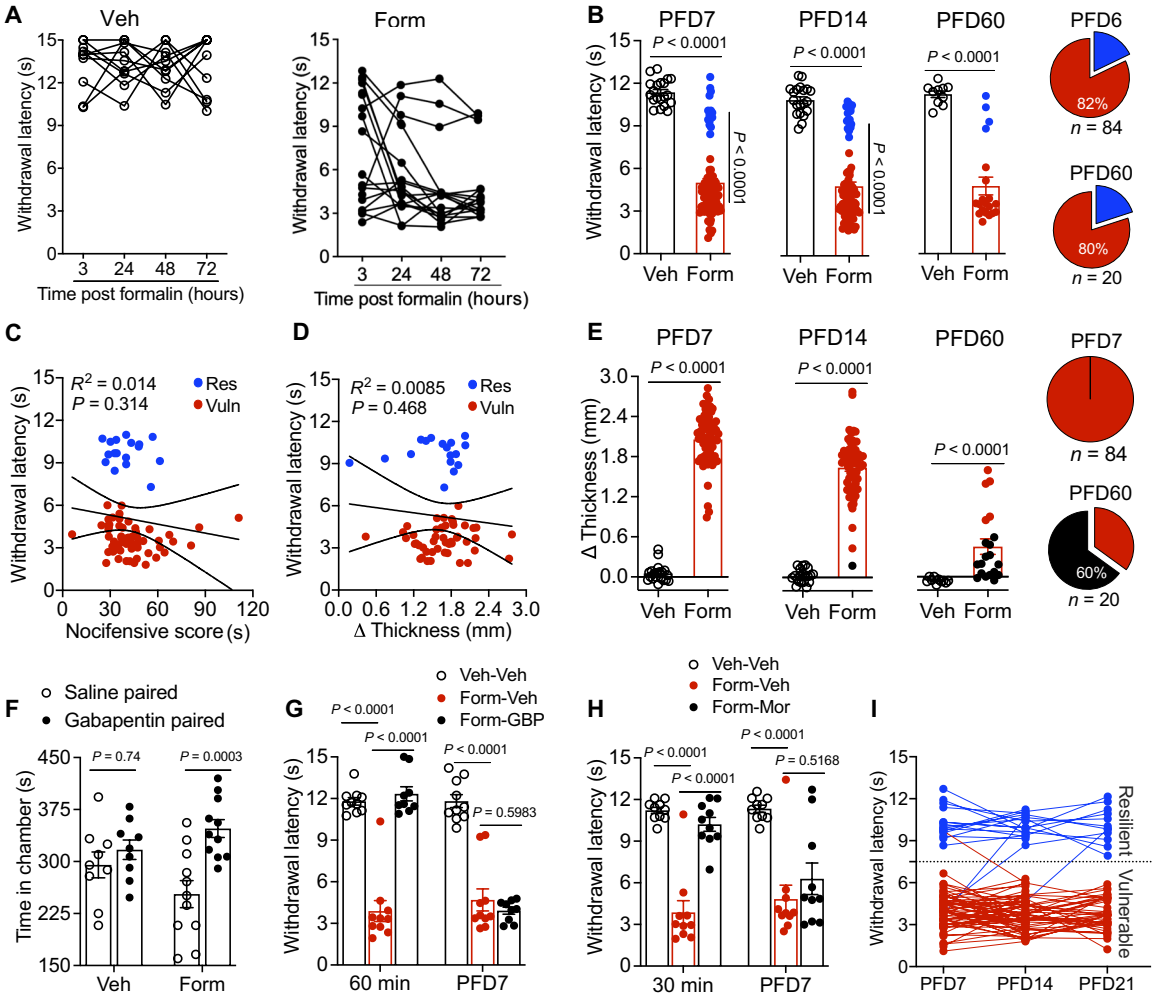

Fig. 1. Chemical end-organ damage produces long-lasting bilateral sensory abnormalities in vulnerable mice. (**A**) Time course of contralateral hyperalgesia assessed 3, 24, 48, and 72 hours after injection of saline (left, $n = 10$) or 1% formalin (right, $n = 15$) in male mice. (**B**) Left: Time course of contralateral hyperalgesia (withdrawal latency, s) in mice given intraplantar injections of saline (Veh, open circles) or 1% formalin (Form, closed circles). Responses in formalin-treated mice did not distribute normally ($K^2 = 37.74$; $P < 0.0001$), and a k-means analysis parsed out two clusters, which were termed "vulnerable" (Vuln, red closed circles) or "resilient" (Res, blue closed circles) based on their susceptibility to the lasting effects of formalin (see fig. S2, G to K). Right: Pie charts showing that the ratio of Vuln versus Res mice remained constant over a 60-day period. PFD, postformalin day. (**C**) Lack of correlation between immediate nocifensive response to formalin (0 to 10 min) and contralateral hyperalgesia assessed on PFD14. (**D**) Lack of correlation between formalin-induced paw edema (Δ thickness, mm) and lasting contralateral hyperalgesia on PFD14. (**E**) Left: Time course of formalin-induced edema. Right: Pie charts showing that edema resolved in 60% of mice over a 2-month period. Inflammation resolution was complete by PFD120 (fig. S1k). (**F**) Intraplantar formalin produced ongoing/spontaneous pain on PFD14 [time in chamber (s) in the conditioned place preference (CPP) test, PFD14]. (**G** and **H**) Contralateral hyperalgesia in formalin-injected animals that had developed hypersensitivity (i.e., Vuln) and were given gabapentin [GBP; 50 mg kg^{-1}, IP; (G)], morphine [Mor; 10 mg kg^{-1}, SC; (H)], or saline (Veh). Tests were conducted 60 min (G; GBP) or 30 min (H; Mor) and 7 days later. (**I**) Segregation between Vuln and Res mice over a 3-week period. Overlaid points are individual animal scores. Results are shown as means ± SEM and were analyzed by a Student's *t* test (F) or two-way analysis of variance (ANOVA) (B, E, G, and H) followed by Bonferroni's post hoc test, as appropriate.

(Fig. 1A) and continued unabated until monitoring was ended (Fig. 1B and fig. S1, C to E). Persistent bilateral hypersensitivity was observed in 100% of female mice (22 of 22) that received formalin (1%) (fig. S1, F to J). The hypersensitive state (i) emerged independently of the intensity of the initial nocifensive response or the ensuing inflammatory reaction, which were comparable across all animals (Fig. 1, C and D); (ii) outlasted the resolution of inflammation, which was complete in 60% of male mice by postformalin day (PFD) 60 (Fig. 1D) and in 100% of male mice by PFD120 (fig. S1K); (iii) was accompanied by lasting spontaneous/ongoing pain, as shown by assessing the ability of the anticonvulsant gabapentin to elicit conditioned place preference (CPP) (Fig. 1F); and (iv) was only temporarily alleviated by gabapentin and morphine (Fig. 1, G and H, and fig. S2, A to F). Last, there was strict segregation between mice that developed sensory abnormalities and those that did not, with minimal exchange occurring between the two groups over a 3-week period (Fig. 1I).

Confirming the emergence of bilateral sensitization, we found that administration of a half-maximal dose of the transient receptor potential cation channel subfamily V member 1 (TRPV1) agonist capsaicin (0.1 μg; Fig. 2A) into the uninjured (contralateral) hind paw evoked stronger nocifensive behavior and bilateral spinal cord

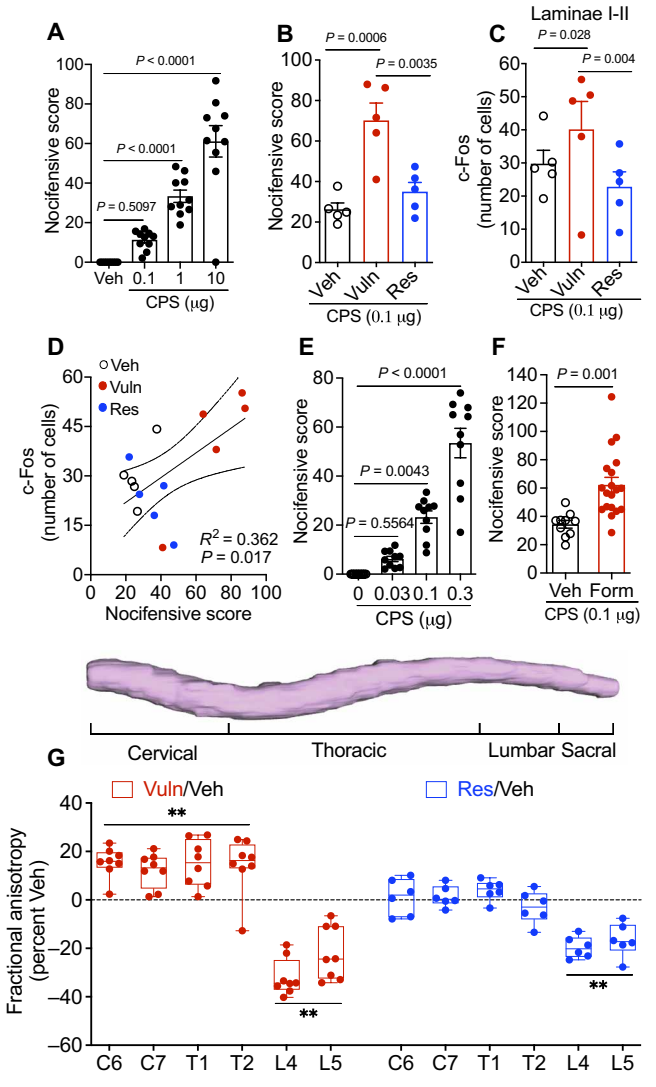

Fig. 2. Chemical end-organ damage produces central sensitization in mouse spinal cord of vulnerable mice. (**A**) Dose-dependent nocifensive responses to intraplantar (hind paw) capsaicin (CPS) injection in naïve mice. (**B**) Effects of CPS (0.1 μg) in mice that had received contralateral injections of saline (Veh, open circles) or formalin (1%, closed circles) 14 days earlier. Formalin-injected mice were tested for contralateral hypersensitivity on PFD14 and were divided into two groups, Vuln (red closed circles) and Res (blue closed circles), as described in Fig. 1B and fig. S2 (G and H). (**C**) Quantification of Fos-like immunoreactive cells in dorsal horn superficial laminae I-II. (**D**) Positive correlation ($R^2 = 0.362$; $P = 0.017$) between nocifensive response to hind paw injection of CPS (0.1 μg) and number of Fos-positive cells in dorsal horn superficial laminae (I-II) in lumbar cord of mice that had previously received formalin in the contralateral hind paw. (**E**) Dose-dependent nocifensive response to forepaw CPS injection in formalin-naïve mice; median effective dose was ~0.1 μg. (**F**) Nocifensive response to contralateral forepaw CPS (0.1 μg) injection in Veh- and Vuln formalin-exposed mice. Results are shown as means ± SEM and were analyzed by Student's *t* test (F) or one-way ANOVA (A, B, C, and E) followed by Dunnett's post hoc test, as appropriate. (**G**) Top: Spinal cord image reconstructed from ex vivo diffusion tensor imaging (DTI) data. Bottom: Fractional anisotropy in spinal cord of Vuln (red circles) and Res (blue circles) mice, assessed at PFD14. Data are expressed as ratio Vuln/Veh and Res/Veh. A total of 21 mice were used in this experiment, and overlaid points are individual animal scores. Means ± SEM. $^{**}P < 0.01$ by two-tailed Student's *t* test with Bonferroni's correction between vehicle-injected (Veh) and Vuln or Res for each spinal cord segment. C, cervical; T, thoracic; L, lumbar. Overlaid points are individual animal scores.

Fos protein expression in animals vulnerable to the lasting effects of formalin, compared with those that either were resilient to such effects or had received only vehicle (Fig. 2, B to D, fig. S3, A to D). Furthermore, two sets of results were suggestive of trans-segmental spreading of sensitization. First, capsaicin injections into the forepaw produced heightened nociception in mice that were previously given formalin in the contralateral hind paw (Fig. 2, E and F). Second, ex vivo diffusion tensor imaging (DTI) experiments revealed substantial alterations in directional water diffusivity—an index of microstructural integrity (*27*) and neural plasticity (*28*)—throughout the spinal cord of formalin-exposed mice (fig. S3, E to G). Most noteworthy, all animals treated with the irritant exhibited lower fractional anisotropy (FA) in the lumbar spinal cord, but only those that became hypersensitive displayed higher FA in cord segments innervating the forelimbs (Fig. 2G).

In persons living with chronic pain, sensory abnormalities are often associated with emotional, cognitive and vegetative disturbances as well as with morphological reorganization of the limbic forebrain (*26*). Similarly, in mice vulnerable to the enduring effects of formalin, thermal and mechanical hypersensitivity was accompanied by heightened anxiety–like behavior (Fig. 3A), defective long-term memory (Fig. 3B), and flattened body-gain trajectory (Fig. 3C). There were also conspicuous alterations in forebrain microstructure. Figure 3 (D and E) illustrates the appearance of bilateral differences in the infralimbic prefrontal cortex and tenia tecta, two gray matter (GM) regions that participate in the control of pain (*29*), memory (*30*, *31*), and stress (Fig. 3, D and E) (*32*, *33*). Moreover, a unilateral volume increase was statistically detectable in the right hippocampal CA2 subfield, which is involved in social memory (*34*), while a trend toward increase ($P = 0.06$) was noted in the right basolateral amygdala, whose role in the emotional dimension of pain is well recognized (Fig. 3D) (*35*). The finding that these alterations were not detectable in resilient formalin-injected mice (Fig. 3, F and G) supports the possibility that they might contribute to the enduring pain-like phenotype exhibited by vulnerable animals. In addition to changes in GM, bilateral volume differences between formalin-exposed (both vulnerable and resilient) and control mice were observed in various fiber tracts, including the anterior commissure, dorsal fornix, and dorsal hippocampal fissure (Fig. 3E). The results show that formalin-induced end-organ damage triggers in susceptible mice the development of a long-lasting neuropathological state whose multimodal manifestations are notably reminiscent of severe chronic pain in humans. For brevity, we will refer to this condition as "chronic pain–like state" (CPLS).

NAAA controls the transition to pain chronicity

We used a genetic loss-of-function/gain-of-function strategy as a first step toward assessing whether NAAA might contribute to the emergence of formalin-induced CPLS. Mice constitutively lacking the enzyme (*36*) displayed normal nociceptive thresholds, motor activity, and feeding patterns (fig. S4, A1 to A6). Nevertheless, formalin (1%) elicited in these mutants a weakened and shorter spontaneous nocifensive response, compared with their wild-type littermates, and did not cause inflammation or persistent hypersensitivity (Fig. 4, A to C, and fig. S4, B1 to B6). Raising the formalin concentration to 3% increased nociceptive responding and evoked pronounced edema and ipsilateral hypersensitivity (fig. S4C1) in NAAA-null mice but still failed to produce lasting contralateral sensitization (Fig. 4, D to F, and fig. S4, C1 to C3). This phenotype

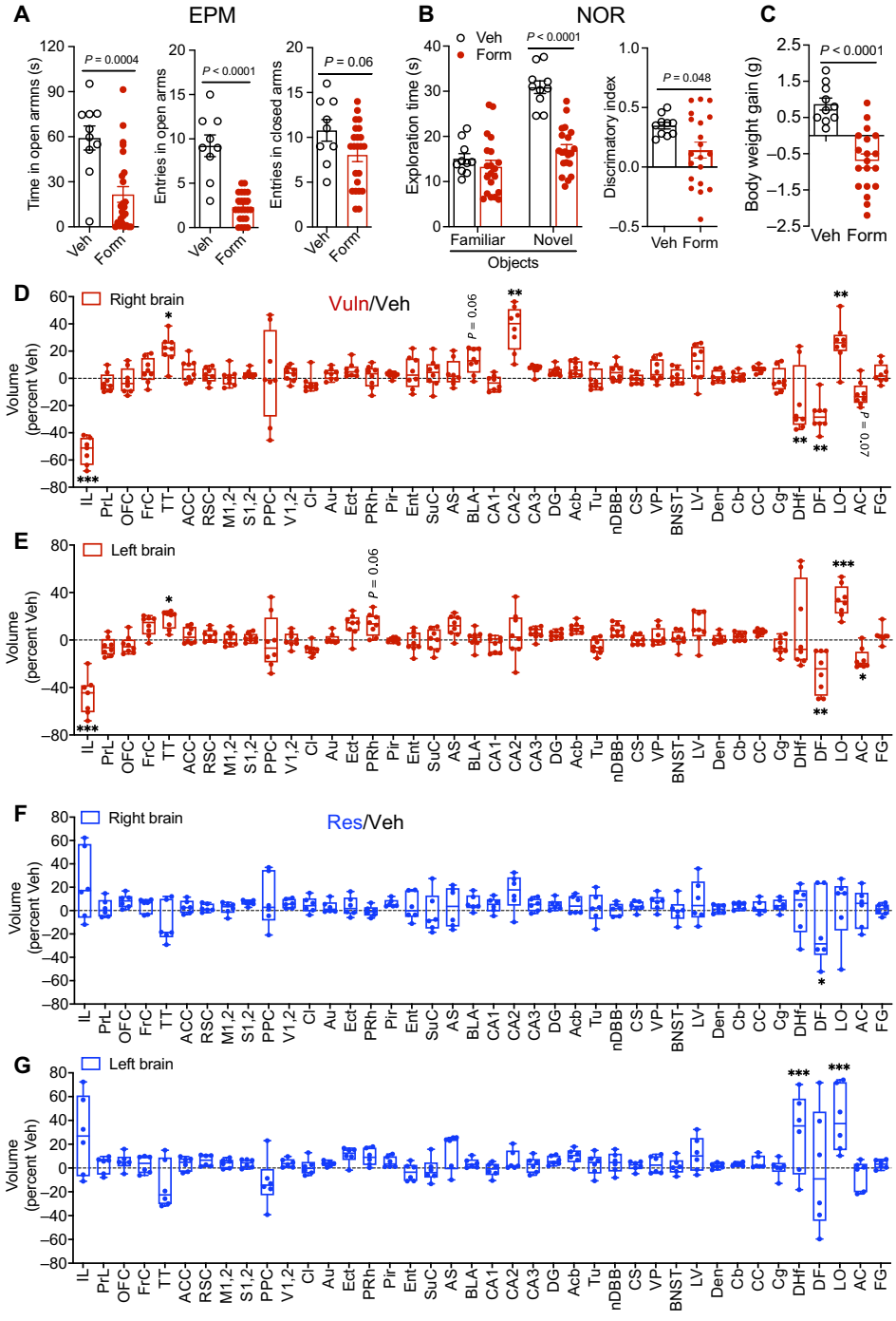

Fig. 3. Formalin injection causes emotional, cognitive, vegetative, and microstructural changes in forebrain of vulnerable mice. (**A**) Anxiety-like behavior in Vuln mice on PFD7 assessed with the elevated plus maze test (EPM). Left, time in open arms (s); center, number of entries in open arms; right, number of entries in closed arms. (**B**) Left: Long-term memory [exploration time (s) in the 24-hour novel object recognition (NOR) test] and discriminatory index (right) in Vuln mice on PFD14. (**C**) Body weight gain in Vuln mice on PFD14. Veh mice, open circles; Vuln mice, red circles. Results are shown as means ± SEM and were analyzed by Student's *t* test [A, B (right), and C] or two-way ANOVA [B (left)] followed by Bonferroni's multiple comparison. (**D** to **G**) Relative volume changes in forebrain structures of Vuln (D and E) and Res (F to G) formalin-treated mice (PFD14). Mice were tested for contralateral hypersensitivity 2 weeks after formalin injection and were divided into Vuln [(D) and (E); red circles] and Res [(F) and (G); blue circles) groups, as described in fig. S2 (G to K). Sixty minutes after testing, the animals were euthanized and processed for ex vivo DTI. (D and F) Regional volume in the right hemisphere; (E and G) regional volume in the left hemisphere. Other diffusion indices [axial diffusivity (AD), radial diffusivity (RD), and FA] are reported in data S2. (D to G) Results are expressed as ratio Vuln/Veh (red circles) and Res/Veh (blue circles). A total of 21 mice were used in this experiment. Means ± SEM. $^{*}P < 0.05$; $^{**}P < 0.01$; $^{***}P < 0.001$ by two-tailed Student's *t* test with Bonferroni's correction between Veh-injected and Vuln or Res for each brain region. AC, anterior commissure; BLA, basolateral amygdala; CA2, hippocampal Cornus Ammonis 2 subfield; DF, dorsal fornix; DHF, dorsal hippocampal fissure; IL, infralimbic prefrontal cortex; LO, lateral olfactory tract; TT, tenia tecta. A complete list of anatomical abbreviations is reported in data S2. Overlaid points are individual animal scores.

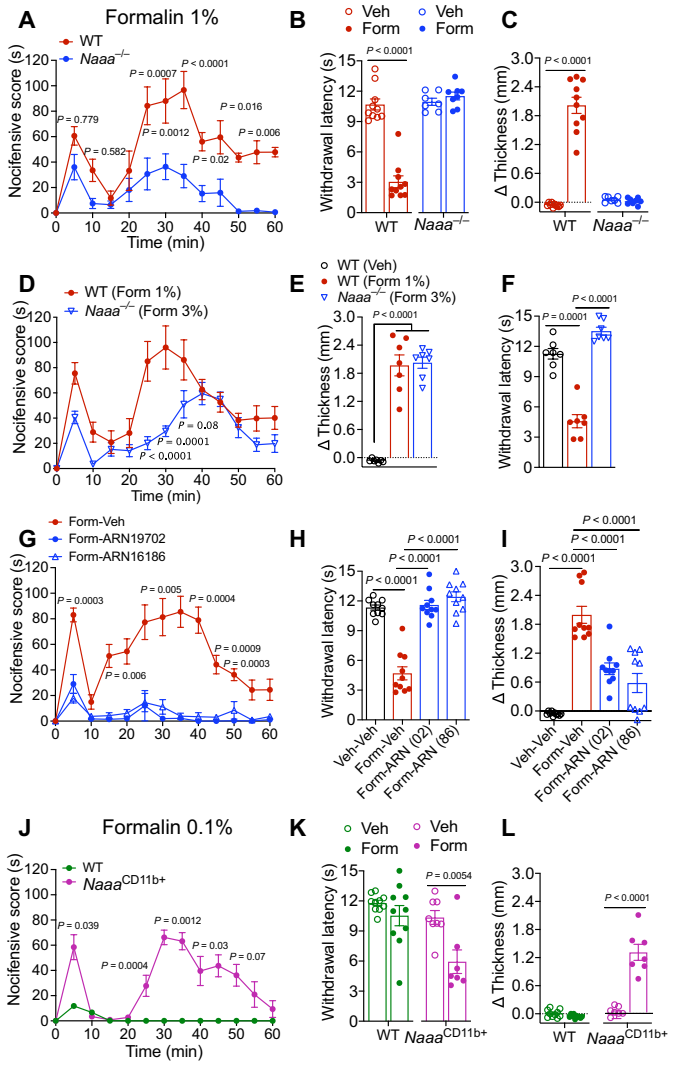

Fig. 4. NAAA controls acute nociception and lasting sensory abnormalities produced by formalin. (**A**) Time course of the response to formalin (1%) in NAAA-null mice (*Naaa*$^{-/-}$, blue circles) and wild-type littermates (WT; red circles). (**B**) Persistent contralateral hyperalgesia, assessed on PFD14, in WT but not *Naaa*$^{-/-}$ mice challenged with 1% formalin. (**C**) Formalin caused paw edema (Δthickness, mm; PFD14) in WT but not *Naaa*$^{-/-}$ mice. Veh, open circles; formalin, closed circles; WT mice, red circles; *Naaa*$^{-/-}$ mice, blue circles. (**D**) Time course of the formalin (1 or 3%) response in *Naaa*$^{-/-}$ (Form 3%) and WT mice (Form 1%). (**E**) Paw edema (PFD14) in WT and *Naaa*$^{-/-}$ mice challenged with 1 and 3% formalin, respectively. (**F**) Persistent contralateral hyperalgesia (PFD14) in WT but not *Naaa*$^{-/-}$ mice injected with 1 and 3% formalin, respectively. Open circles, WT plus Veh; red closed circles, WT plus 1% formalin; blue open triangles, *Naaa*$^{-/-}$ plus 3% formalin. (**G** to **I**) Administration of ARN16186 [ARN (86); 10 mg kg^{-1}, IP], ARN19702 [ARN (02); 30 mg kg^{-1}, IP] prevents (G) nocifensive response, (H) persistent contralateral hyperalgesia (PFD14), and (I) paw edema (PFD14). Open circles, saline plus drug Veh (Veh-Veh); red circles, formalin plus drug Veh (Form-Veh); blue circles, formalin plus ARN19702 [Form-ARN (02)]; blue triangles, formalin plus ARN16186 [Form-ARN (86)]. (**J**) Time course of the response to 0.1% formalin in mice overexpressing NAAA in CD11b^{+} cells (*Naaa*$^{CD11b+}$, magenta) and WT littermates (green). (**K**) Persistent contralateral hyperalgesia in *Naaa*$^{CD11b+}$ exposed to 0.1% formalin (PFD14). (**L**) Paw edema in *Naaa*$^{CD11b+}$ exposed to formalin (0.1%) (PFD14). Veh, open circles; formalin (Form), closed circles; WT mice, red circles; *Naaa*$^{CD11b+}$ mice, magenta circles. Results are shown as means ± SEM and were analyzed by one-way ANOVA (H and I) or two-way ANOVA (A to G and J to L) followed by Dunnett's or Bonferroni's post hoc test.

was recapitulated in wild-type mice by pretreatment with either of two reversible and highly selective NAAA inhibitors: ARN19702 *[30 mg kg^{-1}, intraperitoneally (IP)] and ARN16186 (10 mg kg^{-1}, IP) (Fig. 4, G to I) (*10*). Neither compound affected baseline nociceptive thresholds in naïve animals (fig. S4D). Conversely, mice overexpressing NAAA in CD11b^{+} cells (i.e., monocytes, macrophages, and microglia) (fig. S4, E1 to E6), which play important roles in pain chronification (*3*, *4*), displayed robust nociception, inflammation, and persistent hypersensitivity when challenged with a formalin dose (0.1%) that had negligible impact on control animals (Fig. 4, J to L). The findings suggest that NAAA facilitates acute defensive reactions to injury and point to a possible role for the enzyme in the development of formalin-induced CPLS.

To delineate such a role, we administered ARN19702 (30 mg kg^{-1}, IP) or its vehicle to male mice once daily for three consecutive days starting 24 hours after the formalin challenge and evaluated sensory, cognitive, emotional, vegetative, and microstructural outcomes during the following 2 weeks. Despite its short duration, treatment with the NAAA inhibitor effectively halted CPLS consolidation, normalizing evoked hypersensitivity and ongoing pain, anxiety-like behavior, memory deficits, and body weight gain (Fig. 5, A to E, and data S1) and reversing CPLS-associated changes in spinal and forebrain DTI measures (Fig. 5, F and G; fig. S5, A to F; and data S2). Furthermore, the protective effects of ARN19702 were mimicked by a second NAAA inhibitor, ARN16186 (10 mg kg^{-1}, IP) (Fig. 5A and fig. S6, A to C), and were not sex dependent (Fig. 5H and fig. S6, D to G).

Unlike agents that interfere with NAAA activity, maximally effective dosages of four mechanistically distinct analgesic and anti-inflammatory drugs—gabapentin (50 mg kg^{-1}, IP), morphine [10 mg kg^{-1}, subcutaneously (SC)], ketamine (4 mg kg^{-1}, IP), and ketoprofen (100 mg kg^{-1}, IP)—failed to stop the conversion to CPLS when administered on PFD2 to PFD4 (Fig. 5, I to L, and fig. S6, H to K). In addition, even though NAAA blockade attenuates inflammation in rodent models (*9*), the 3-day ARN19702 regimen had no detectable influence on paw edema (Fig. 5M), likely owing to its brief duration. We interpret these findings as indicating that NAAA inhibitors halt the transition to pain chronicity through a mechanism that is distinguishable from their antinociceptive and anti-inflammatory properties. To mark this distinction, we will refer to such mechanism as "algostatic"—from the ancient Greek ἄλγος "pain" and ἱστάναι "to stop."

To determine whether the algostatic effects of NAAA inhibition could be generalized to other models of persistent pain, we asked whether ARN19702 might affect the development of hypersensitivity, spontaneous pain, and cognitive abnormalities in mice subjected to chronic constriction injury (CCI) of the sciatic nerve (*37*). We loosely tied the nerve under anesthesia and, starting 24 hours later, administered ARN19702 (30 mg kg^{-1}, IP) or its vehicle once daily for 3 days. Spontaneous pain and hypersensitivity to heat and mechanical stimuli were assessed on postoperative days (POD) 7 to 14, and long-term memory was assessed on POD26. Treatment with the NAAA inhibitor prevented the appearance of all chronic pain manifestations (Fig. 6, A to D). As expected from prior results (Fig. 4, A to F), genetic NAAA deletion also blocked the development of thermal and mechanical hypersensitivity (Fig. 6, E and F, and data S3). We conclude that postinjury NAAA removal interrupts the emergence of CPLSs elicited in mice by either chemical or mechanical tissue damage.

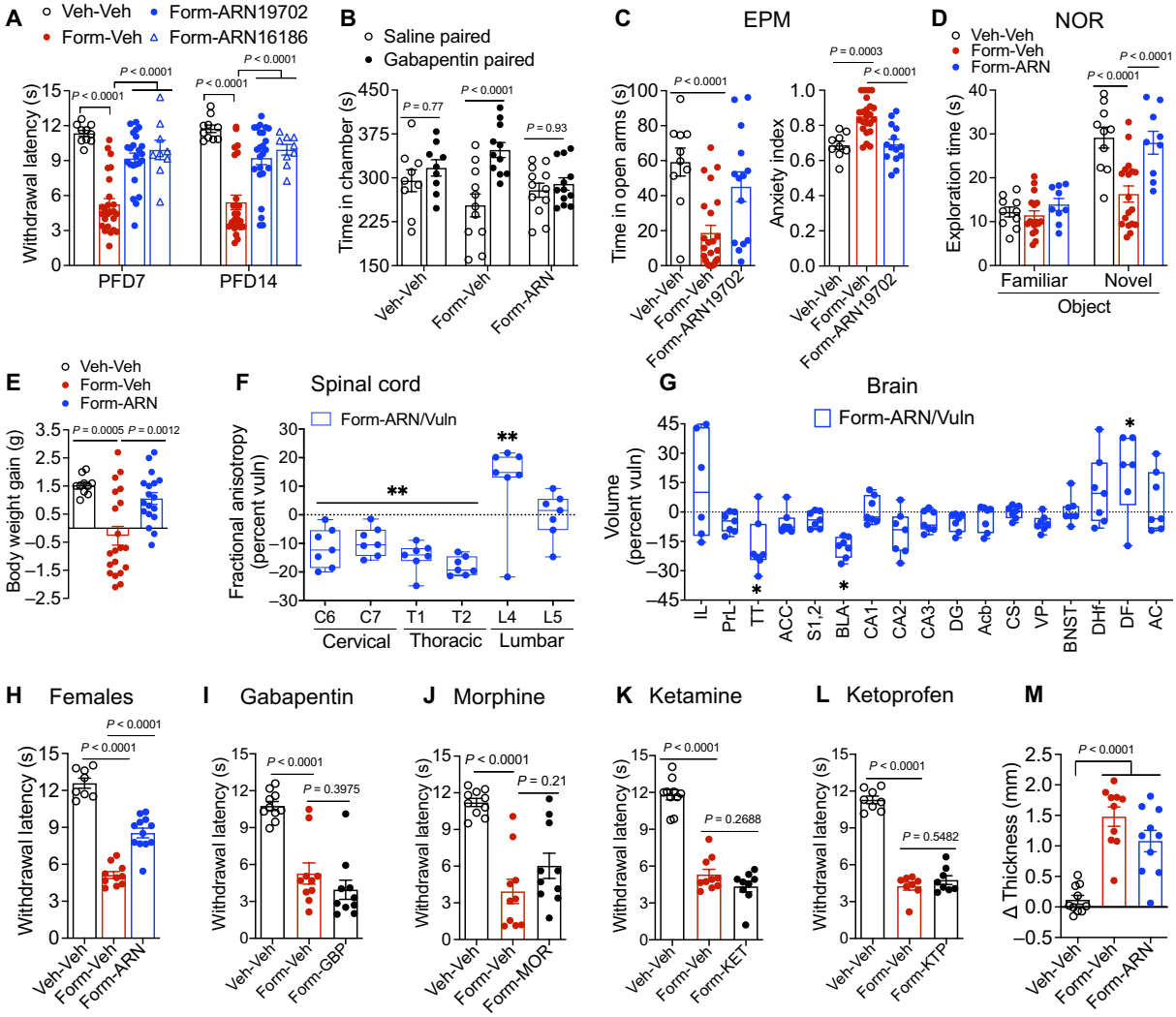

Fig. 5. NAAA inhibition halts the emergence of formalin-induced CPLS. (**A**) Time course of contralateral hyperalgesia in formalin-injected male mice that received ARN19702 (30 mg kg^{-1}, IP; blue circles), ARN16186 (10 mg kg^{-1}, IP; blue triangles), or Veh (open circles) once daily from PFD1 to PFD3. (**B**) Effects of postformalin ARN19702 (30 mg kg^{-1}, IP) administration (PFD1 to PFD3) on spontaneous/ongoing pain response [time in chamber (s) during the CPP test, PFD14]. (**C** to **E**) Effects of postformalin ARN19702 administration (PFD1 to PFD3) on (C) anxiety-like behavior [(right) time in open arms (s) of an EPM and (left) anxiety index, PFD7]; (D) long-term memory [exploration time (s) in the 24-hour NOR test, PFD14]; (E) body weight gain (PFD14); (**F**) FA in spinal cord (PFD14); and (**G**) volume changes in forebrain (PFD14); data in (F) and (G) are from Vuln formalin-injected mice and are expressed as ratio ARN19702-treated/untreated animals. (**H**) Contralateral hyperalgesia in formalin-injected female mice that received ARN19702 (30 mg kg^{-1}, IP; blue circles) or Veh (open circles) once daily from PFD1 to PFD3. (**I** to **L**) The analgesics GBP [50 mg kg^{-1}, IP, (I)], MOR [10 mg kg^{-1}, SC, (J)], ketamine [KET; 4 mg kg^{-1}, IP, (K)], and ketoprofen [KTP; 100 mg kg^{-1}, IP, (l)] (administered on PFD1 to PFD3) do not prevent contralateral hyperalgesia (PFD14) in WT mice treated with formalin. (**M**) Paw edema (Δthickness, mm; PFD14) in male mice treated with formalin, formalin plus ARN19702, or their Veh. Results are expressed as means ± SEM and were analyzed by one-way ANOVA (B, C, E, and H to M) or two-way ANOVA (A and D) followed by Dunnett's or Bonferroni's post hoc test, as appropriate. Overlaid points are individual animal scores. *$P < 0.05$ and **$P < 0.01$.

A critical period for pain chronification

The ability of NAAA inhibitors to stop CPLS consolidation was crucially dependent on the timing of their administration. This was demonstrated by the experiment illustrated in Fig. 7 (A and B) (data S4), in which a single injection of ARN19702 (30 mg kg^{-1}, IP) was administered to separate groups of male wild-type mice on PFD1, 5, 6, 7, 8, or 9. The NAAA inhibitor provided full protection when given once on PFD3 or PFD4 but had no such effect when given on PFD1 or PFD5 to PFD9 (Fig. 7B)—although at all time points, it temporarily attenuated pain behaviors (fig. S6, L to O). Administration on PFD2 was partially effective. The time window for NAAA inhibitor efficacy coincided with a transient rise in *Naaa* gene transcription in the lumbar (L4–L6) spinal hemicord ipsilateral to the injured paw, which was maximal at PFD3 (Fig. 7C, left). No change occurred on the contralateral side, where *Naaa* mRNA content remained stable from PFD1 to PFD5 (Fig. 7C, right). The spike in *Naaa* transcription was associated with higher levels of immunoreactive NAAA (Fig. 7, D to G) and with a reduction in local PEA levels (Fig. 7H). Colocalization studies showed that immunoreactive NAAA was primarily localized to NeuN$^+$ cells (neurons) of the dorsal and ventral horns (Fig. 7, E to G), although sparse Olig2-positive cells (oligodendrocytes) were also detected (fig. S7).

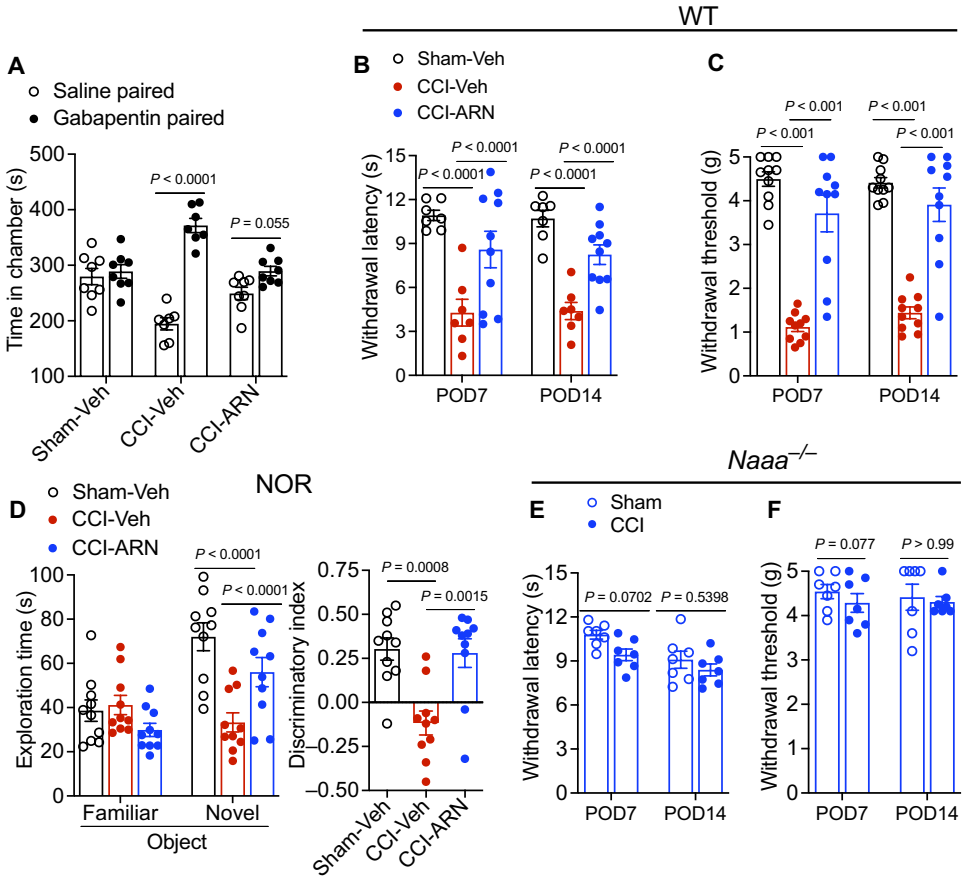

Fig. 6. NAAA blockade prevents lasting sensory and cognitive abnormalities produced by CCI. (**A**) Effects of post-CCI ARN19702 (30 mg kg^{-1}, IP) administration (PFD1 to PFD3) on spontaneous/ongoing pain response [time in chamber (s) during the CPP test, POD14]. (**B**, **C**, **E**, and **F**) Time course of ipsilateral hyperalgesia (B and E) and allodynia (C and F) after sham surgery (open circles) or sciatic nerve ligation (CCI, closed circles). (B and C) WT mice subjected to CCI and treated with Veh (red circles) or ARN19702 (30 mg kg^{-1}, IP; blue circles). (**D**) Long-term memory in WT mice that were subjected to sham or CCI surgery and received either ARN19702 or its Veh. Left: Exploration time (s) in the 24-hour NOR test on POD26. Right: Discriminatory index. (E and F) *Naaa*$^{-/-}$ mice subjected to CCI or sham surgery without drug treatment. Results are expressed as means ± SEM and were analyzed by one-way ANOVA (D, right) or two-way ANOVA [B, C, D (Left), E, and F] followed by Dunnett's or Bonferroni's post hoc test, as appropriate. Overlaid points are individual animal scores.

Accrued spinal cord NAAA activity was required for the induction of persistent hypersensitivity elicited by formalin or CCI, as this was stopped by postinjury intrathecal infusion of either ARN19702 or ARN077, a covalent NAAA inhibitor that does not cross the blood-brain barrier (Fig. 7, I and J, and data S5) (*9*). In sum, the results show that end-organ damage sets off a transitory suppression of NAAA-regulated PEA signaling in innervating segments of the spinal cord, which starts 24 to 48 hours after the injury, lasts approximately 72 hours and is required for pain to become chronic.

Transcriptomic and metabolomic experiments offer important insights into the molecular events unfolding during this critical period. RNA sequencing analyses of L4–L6 spinal cord fragments ipsilateral to the formalin injection site identified large-scale transcriptional changes at PFD3 and PFD4 compared with time- and site-matched controls (Fig. 8A and data S6). At PDF4, when changes were largest, differentially up-regulated transcripts were substantially enriched in the following Gene Ontology (GO) categories: synaptic membrane [adjusted *P* value (P_{adj}) = 1.17^{-35}], neuron-to-neuron synapse (P_{adj} = 7.82^{-30}), postsynaptic membrane (P_{adj} = 8.42^{-30}), glutamatergic synapse (P_{adj} = 8.40^{-27}), and axon development (P_{adj} = 2.53^{-26}) (fig. S8A and data S11). Notably, expression of neuronal genes encoding for, among others, voltage-gated sodium channels (e.g., *Scn1a* and *Scn8a*), calcium channels (e.g., *Cacn1a* and *Cacn1b*), and α-amino-3-hydroxy-5-methyl-4-isoxazole propionic acid (AMPA) receptor–regulating proteins (e.g., *Cacng2* and *Cacng5*) was strongly enhanced (Fig. 8B and data S11). Transcription of key components of cholesterol biosynthesis (e.g., *Hmgcr* and *Hmgcs2*)—a requisite for membrane biogenesis (*38*, *39*)—was also heightened (Fig. 8C). These changes are consistent with evidence of widespread synaptic (*16*) and proteomic (*40*) modifications in spinal cord of animals experiencing chronic pain states. By contrast, differentially down-regulated transcripts at PFD4 were enriched in categories including mitochondrial protein complex (P_{adj} = 3.93^{-69}), inner mitochondrial membrane protein complex (P_{adj} = 4.03^{-47}), and mitochondrial respiratory chain (P_{adj} = 2.01^{-32}) (fig. S8B). Accordingly, many protein components of tricarboxylic acid (TCA) cycle and oxidative phosphorylation were suppressed on PFD4 (Fig. 8D). The opposite occurred, however, with two members of the bifunctional 6-phosphofructo-2-kinase fructose-2,6-biphosphatase (*Pfkfb*) family (*Pfkfb3* and *Pfkfb4*) and with the glucose transporter Glut1 (*Slc2a12*) (Fig. 8E and data S6). Notably, *Pfkfb3* shunts glucose toward glycolysis, whereas *Pfkfb*4 redirects glucose toward the

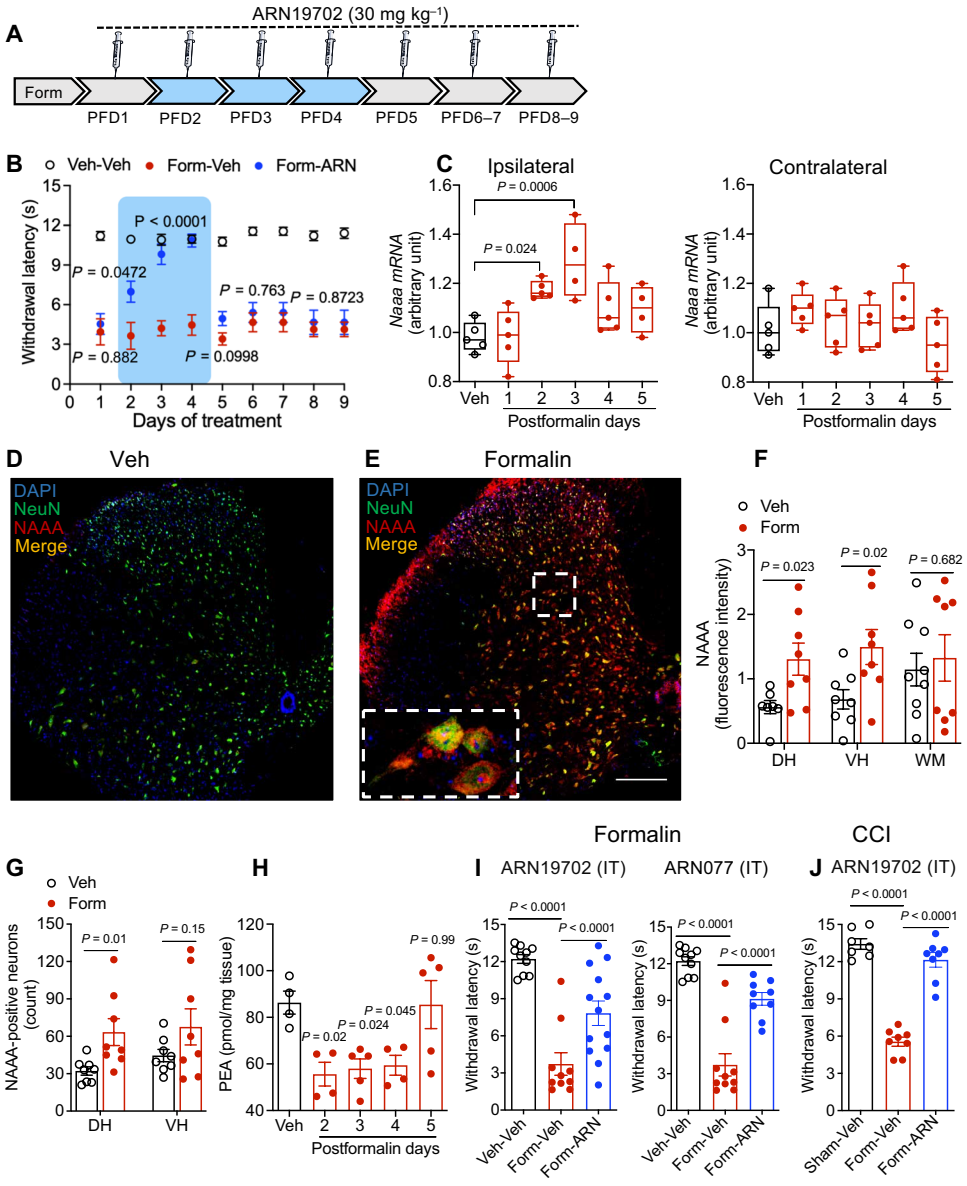

Fig. 7. A critical period for pain chronification. (**A**) Mice received formalin (1%) or saline and were assigned to seven groups ($n = 10$ mice each): five received one dose of ARN19702 (30 mg kg^{-1}, IP) or Veh on PFD1 or PFD2 to PFD5; two additional groups received one daily dose of ARN19702 or Veh on PFD6–7 or PFD8–9. Contralateral hyperalgesia was assessed 2 weeks later. (**B**) Effects of ARN19702 (blue) or Veh (red) on CPLS establishment. Open circles, no formalin. (**C**) Time course of *Naaa* transcription in ipsilateral (left) or contralateral (right) L4–L6 hemicord of mice treated with Veh (open circles) or formalin (red circles). (**D** to **G**) Localization of immunoreactive NAAA (irNAAA) in ipsilateral L4–L6 hemicord of (D) Veh- and (E) formalin-injected mice (PFD4). NAAA partially colocalized with NeuN; other markers are shown in fig. S7. Magnification: ×10 (D and E) or ×40 [(E, bottom), zoom 2×]. Scale bar, 20 μm. DAPI, 4′,6-diamidino-2-phenylindole. (F) Quantification of irNAAA in ipsilateral dorsal horn (DH), ventral horn (VH), and white matter (WM) in L5 cord of Veh- or formalin-injected mice. (G) Quantification of NAAA-immunoreactive NeuN$^+$ cells in ipsilateral DH and VH in L5 cord of Veh- or formalin-injected mice. (**H**) PEA levels in ipsilateral L4–L6 hemicord fragments of Veh- (open circles) or formalin-treated mice (red circles) (PFD4). (**I**) Effects of intrathecal ARN19702 or ARN077 (30 ng, 5 μl) at PFD2 and PFD4 on hypersensitivity at PFD14. (**J**) Effects of intrathecal ARN19702 at POD2 and POD4 on hypersensitivity at POD14. Veh, empty circles; formalin, red circles; NAAA inhibitors, blue circles. Means ± SEM of $n = 4$ to 10 mice per group. Student's t test with Bonferroni's correction (G), one-way ANOVA (B, C, and H to J) or two-way ANOVA (A) followed by Dunnett's or Bonferroni's post hoc test.

pentose phosphate pathway, suggesting that both processes might be activated during the critical period for CPLS development (*41*).

The transcriptional shift was paralleled by a largely concordant set of metabolomic changes (Fig. 8F and data S7). Decreased concentrations of free amino acids (Fig. 8G) and nonesterified unsaturated fatty acids (Fig. 8H) together with increased cholesterol and phospholipid precursors (zymosterol and *sn*-glycerol-3-phosphate, respectively) (Fig. 8H) support the possibility that protein synthesis and membrane biogenesis are accelerated on PFD4. Concomitantly, *N*-acetyl-L-aspartate, which provides carbon units for neural lipid biosynthesis (*42*), was increased (Fig. 7G), whereas urea cycle intermediates ornithine and citrulline declined (Fig. 8I), possibly reflecting accrued nitrogen recycling (*43*). Furthermore, elevated glucose, glucose-1-phosphate (G1P), glucose-6-phosphate (G6P),

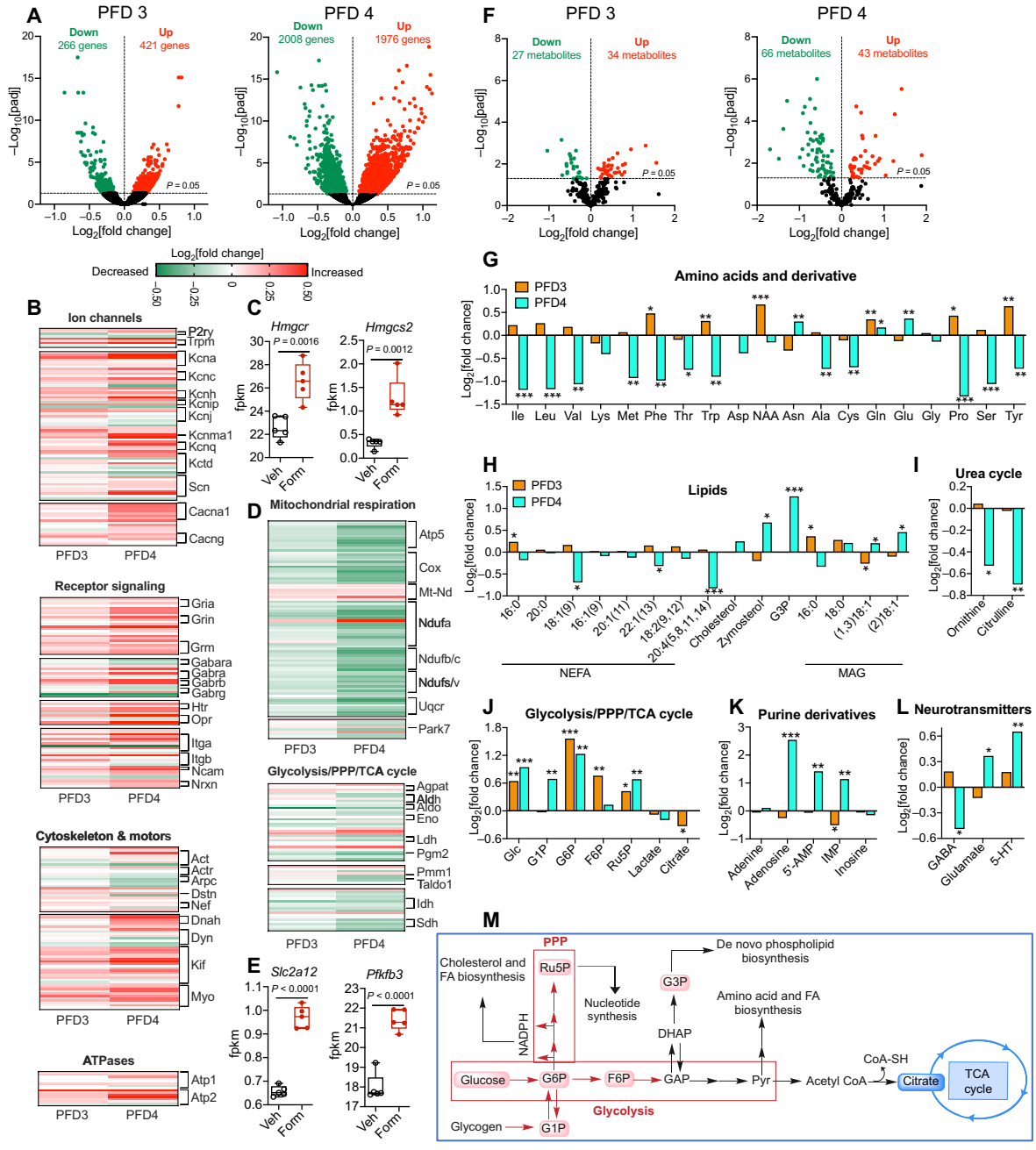

Fig. 8. The critical period for pain chronification coincides with a broad reprogramming of spinal cord metabolism. (**A**) Volcano plots showing changes in gene transcription at PFD3 (left) and PFD4 (right) in lumbar spinal hemicord (L4–L6) ipsilateral to the injection site. Green, differentially down-regulated transcripts; red, differentially up-regulated transcripts. (**B**) Heatmaps showing expression of genes encoding for ion channels, neurotransmitter receptors/ancillary proteins, cytoskeletal/motor proteins, and ATPases. (**C**) Transcription of cholesterol biosynthesis constituents hydroxymethyl glutaryl-CoA reductase (*Hmgcr*) and hydroxymethyl glutaryl-CoA synthase (*Hmgcs2*), assessed at PFD4. (**D**) Heatmaps showing expression of mitochondrial respiration and tricarboxylic acid (TCA) cycle genes. (**E**) Transcription of glucose transporter Glut1 (*Slc2a12*) and phosphofructokinase (*Pfkfb-3*) at PFD4. (**F**) Volcano plots showing changes in core metabolism constituents at PFD3 (left) and PFD4 (right) in ipsilateral L4–L6 hemicord. Green, decreased metabolites; red, increased metabolites. (**G**) Free amino acids, including *N*-acetyl-L-aspartate; (**H**) nonesterified fatty acids (NEFA; identified by their short-hand notation) and other lipids [cholesterol, zymosterol, and monoacylglycerols (MAG)]; and (**I**) urea cycle intermediates. (**J**) Glycolytic, pentose phosphate pathway (PPP), and TCA cycle intermediates: glucose (Glc), glucose-1-phosphate (G1P), glucose-6-phosphate (G6P), fructose-6-phosphate (F6P), and ribulose-5-phosphate (Ru5P). (**K**) Purine derivatives including the energy crisis markers 5′-adenosine monophosphate (AMP) and 5′-inosine monophosphate (IMP). (**L**) Neurotransmitters γ-aminobutyric acid (GABA), glutamate, and 5-hydroxytryptamine (5-HT). (**M**) Summary of observed metabolic changes: red, up-regulated metabolites; blue, down-regulated metabolites. The changes are consistent with accrued glucose transport (glucose), glycogenolysis (G1P), glycolysis (G6P and F6P), and pentose phosphate catabolism (Ru5P), and with decreased TCA cycle (citrate). Glycolysis-derived pyruvate (Pyr) and PPP-derived NADPH (reduced form of nicotinamide adenine dinucleotide phosphate) may be used for protein and lipid biosynthesis. GAP, glyceraldehyde 3-phosphate; DHAP, dihydroxyacetone 3-phosphate. Five mice per group were used for RNA sequencing, and 12 mice per group were used for metabolomic analyses. **P* < 0.05; ***P* < 0.01; ****P* < 0.001, Student's *t* test with Bonferroni's correction.

fructose-6-phosphate (F6P), and ribulose-5-phosphate (Ru5P) at PFD3 and/or PFD4 (Fig. 8J) were suggestive of up-regulated glucose transport, glycogenolysis (G1P), glycolysis (G6P and F6P), and the oxidative branch of the pentose phosphate pathway (Ru5P). The small but notable decrease in citric acid on PFD3 (Fig. 8J) was consistent with reduced TCA cycle activity, while unchanged lactate levels suggested that glycolysis-derived pyruvate (which was undetectable in our samples) may have been used for biosynthetic needs. Together, the above alterations may account for the rise in 5′-adenosine monophosphate (AMP) and 5′-inosine monophosphate (IMP) (Fig. 8K), two nucleotides that accumulate in cells during energy crises (*44*). Last, the neurotransmitters glutamate and 5-hydroxytryptamine were increased, whereas γ-aminobutyric acid was decreased (Fig. 8L), possibly due to imbalanced excitation/inhibition and enhanced descending serotonergic input (*16*). Thus, the critical period for the consolidation of formalin-induced CPLS coincides with a transcriptionally controlled metabolic switch from mitochondrial respiration to aerobic glycolysis (Fig. 8M), which is localized to spinal cord segments that receive direct nociceptive input from the lesioned paw. Systemic ARN19702 administration on PFD2 to PFD3 prevented the appearance of transcriptional and metabolic changes on the following day (fig. S8, C, D, and G to K, and data S11), demonstrating a critical role for NAAA in enabling this switch.

NAAA governs pain chronification via PEA signaling at PPAR-α

As noted above, PEA levels in ipsilateral lumbar spinal cord (L4–L6) of formalin-injected mice were markedly reduced on PFD4, compared with vehicle-treated controls (Fig. 9A). Postformalin ARN19702 administration normalized such levels (Fig. 9A), suggesting that PPAR-α—which is expressed in neurons (*11*, *45*) and other cells of the central nervous system (*45*)—might mediate the algostatic effects of NAAA inhibition. Experiments with mice constitutively lacking the nuclear receptor confirmed this possibility. When challenged with either 0.1 or 1% formalin, PPAR-α–null mice exhibited substantially stronger nociception compared with wild-type controls (Fig. 9, B and E), which gave way at both doses to inflammation (Fig. 9, C and F) and lasting hypersensitivity (Fig. 9, D and G, and data S8). In these mutants, the transition to CPLS was unaffected by ARN19702 (30 mg kg^{-1}, IP) (Fig. 9H and data S9), a trait that was replicated in wild-type animals by pretreatment with the selective PPAR-α antagonist GW6471 (4 mg kg^{-1}, IP) (Fig. 9I). Further supporting a pivotal role for PPAR-α in gating pain chronification, we found that postinjury administration of the highly potent and selective PPAR-α agonist GW7647 (10 mg kg^{-1}, IP) stopped this process in three different experimental settings: (i) wild-type mice treated with 1% formalin (Fig. 9J), (ii) NAAA–overexpressing mice treated with 0.1% formalin (Fig. 9K), and (iii) wild-type mice subjected to CCI (Fig. 9L and data S10). Like NAAA inhibition, PPAR-α activation by GW7647 prevented injury-associated changes in spinal cord transcription (fig. S8, E and F, and data S11). Last, CPLS was blocked by exogenous PEA (30 mg kg^{-1}, SC) but not by the weak PPAR-α agonist fenofibrate (100 mg kg^{-1}, IP) (Fig. 9, M and N, and data S10), which is used in the clinic to treat hyperlipidemia.

DISCUSSION

Twenty percent of the adult world population—approximately 1.5 billion people—suffer from chronic pain (*46*, *47*), yet its

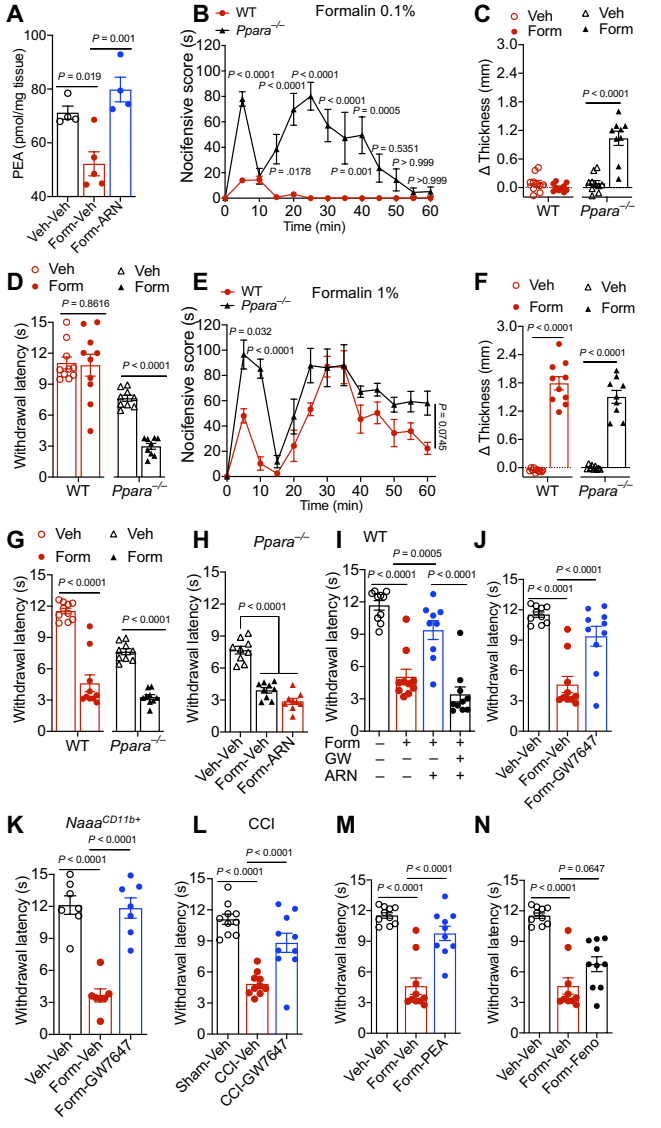

Fig. 9. NAAA controls the transition to pain chronicity via PEA signaling at PPAR-α. (**A**) PEA content in ipsilateral lumbar cord (L4–L6) in mice treated with intraplantar saline (Veh, open circles) or formalin (Form, closed circles) and then with ARN19702 (30 mg kg^{-1}, IP; blue circles) or its Veh (red circles) on PFD2 to PFD4. Mice were euthanized for lipid analysis 2 hours after ARN19702 administration. (**B** to **D**) Effects of intraplantar formalin (0.1%) injection on (B) acute nocifensive behavior, (C) paw edema [Δthickness, mm; PFD14], and (D) contralateral hyperalgesia (withdrawal latency, s; PFD14) in *Ppara*$^{-/-}$ (red triangles) or WT mice (green circles). (**E** to **G**) Effects of formalin (1%) on (E) acute nocifensive behavior, (F) paw edema (PFD14), and (G) contralateral hyperalgesia (PFD14) in *Ppara*$^{-/-}$ and WT mice. (**H** and **I**) Contralateral hyperalgesia (PFD14) in (H) *Ppara*$^{-/-}$ mice after administration of ARN19702 and (I) WT mice after administration of ARN19702 plus PPAR-α antagonist GW6471 (4 mg kg^{-1}, IP, 15 min before ARN19702). (**J** to **L**) Contralateral hyperalgesia after administration of PPAR-α agonist GW7647 (10 mg kg^{-1}, IP) on postprocedural days 2 to 4 in (J) WT mice exposed to 1% formalin, (K) NAAA-overexpressing mice (*Naaa*$^{CD11b+}$) exposed to 0.1% formalin, and (L) WT mice subjected to sciatic nerve ligation (CCI). (**M** and **N**) Effects of administration of (M) PEA (30 mg kg^{-1}, IP) or (N) fenofibrate (Feno, 100 mg kg^{-1}, IP, closed circles) on PFD2 to PFD4. Overlaid points are individual animal scores. Means ± SEM of $n = 4$ to 10 mice per group. *$P < 0.05$; **$P < 0.01$; ***$P < 0.001$ by one-way ANOVA (A and H to N) or two-way ANOVA (B to G) followed by Dunnett's or Bonferroni's post hoc test, as appropriate.

management continues to depend on a handful of analgesic drug classes, such as the opioids, which have dubious long-term effectiveness and can cause addiction (*48*). Epidemiological studies indicate that chronic pain is a major risk factor for opioid use disorder, with more than 60% of people who misused the drugs reporting to have done so to achieve pain relief (*49*). The development of chronic pain is often associated with accidental or surgical tissue trauma. For example, a review of five independent surveys found that more than half of patients who underwent thoracotomy reported experiencing pain 1 year after surgery, while 21% were still in pain 7 years later (*1*). Nerve damage may contribute to pain chronification after physical trauma, but the sequence of events underlying this process—including its molecular and cellular components, timing, and anatomical localization—remains largely unknown (*1*, *5*). In the present report, we show that NAAA-regulated PEA signaling at PPAR-α is a critical control point in the transition to chronic pain after tissue injury, which can be effectively targeted by small-molecule therapeutics. Using two distinct experimental models, one of which is fully characterized here, we found that disabling intracellular NAAA activity in spinal cord during a brief critical period after end-organ damage forestalls the emergence of chronic pain by reprogramming local metabolism from aerobic glycolysis to mitochondrial respiration. The results identify NAAA and its cognate signaling complex as a molecular target for the prevention of chronic pain consolidation following a traumatic injury.

As we set out to examine NAAA's possible roles in the progression to pain chronicity, we selected two models—intraplantar formalin injection and CCI of the sciatic nerve—that would allow us to capture this transition. In the formalin test, which was originally developed to investigate acute nociceptive responses to tissue injury (*18*), subcutaneous injection of this irritant produces a nocifensive reaction that lasts approximately 60 min and is followed by localized inflammation and persistent hypersensitivity to heat and pressure (*19*, *20*, *50*). Our current studies indicate that this lasting state (abbreviated here as CPLS) closely retraces key manifestations of severe chronic pain in humans, including spontaneous pain; bilateral and trans-segmental spreading of sensitization (*21*, *22*, *51*); disturbances in emotional, cognitive, and vegetative function (*23*, *24*, *52*, *53*); and reorganization of forebrain areas involved in the control of stress and emotion (e.g., prefrontal cortex and basolateral amygdala) (*25*, *26*, *54*). While some of these abnormalities have been described in neuropathic pain models such as CCI (e.g., increased anxiety–like behaviors and memory deficits) (*55*), others have not (e.g., extraterritorial spreading of sensitization). Moreover, our results show that CPLS emerges independently of the inflammatory reaction to formalin (Fig. 1, C to E) and outlasts the resolution of inflammation (Fig. 1E), ostensibly aligning the tail-end of this model with human pathologies in which pain is the sole complaint (*56*). Despite these useful features, which warrant further evaluation, formalin-induced CPLS has no face validity as a model to study persistent pain produced by accidental or surgical trauma, a common root cause of this condition (*1*). For this reason, we also used the CCI model, a well-established paradigm in which mechanical damage to the sciatic nerve results in lasting sensory, emotional, and cognitive abnormalities (*55*). Despite their differences, the two models yielded comparable responses to pharmacological or genetic interventions targeting NAAA-regulated PEA signaling.

Preclinical evidence points to NAAA as a potential target for analgesic and anti-inflammatory therapy (*10*, *57*). In peripheral tissues, where the functions of PEA are better understood (*58*, *59*), sensory neurons of the dorsal root ganglia (DRG), tissue-resident macrophages, and other host-defense cells generate this lipid mediator in amounts that are sufficient to maintain PPAR-α in an activated state. Following tissue damage, danger signals such as bacterial endotoxin initiate a molecular program that lowers PEA production and heightens NAAA-catalyzed PEA degradation, resulting in an overall reduction in PPAR-α–mediated signaling and a consequent enhancement of the inflammatory response (*60*). Consistent with this scenario, NAAA inhibitors and PEA display comparable antinociceptive and anti-inflammatory properties in animal models. For example, topical application of the covalent NAAA inhibitor *(S)*-OOPP reinstates normal PEA levels in activated leukocytes and blunts inflammatory responses induced by carrageenan or endotoxin (*60*). Similarly, the β-lactone derivative ARN077, which also inhibits NAAA covalently, corrects sensory abnormalities caused in mice and rats by carrageenan injection, ultraviolet B radiation, or CCI (*61*). These effects are mimicked by exogenous PEA, are absent in PPAR-α–null mice, and are prevented, in rats, by the selective PPAR-α antagonist GW6471 (*61*). Furthermore, ARN077 reduces mechanical hypersensitivity in fibrosarcoma-bearing mice and rapidly normalizes calcium signaling in DRG neurons cocultured with fibrosarcoma cells (*62*). Confirming its proposed mechanism of action, ARN077 restores baseline PEA levels in diseased tissues of CCI (*61*) and tumor-bearing mice (*62*). Other chemically and mechanistically different NAAA inhibitors exert similar effects (*10*). For example, the noncovalent agent ARN19702 suppresses nociceptive behavior evoked by formalin or CCI as effectively as does ARN077, which acts via covalent modification (*63*). A meta-analysis commissioned by the International Association for the Study of Pain recently noted that NAAA inhibitors "produced the largest significant attenuation of pain-associated behavior compared to control" among all endocannabinoid- and cannabinoid-related agents reported in the preclinical literature (*57*). Although PEA-dependent recruitment of PPAR-α is required for the rapid antinociceptive properties of NAAA inhibitors, the mechanism through which activated PPAR-α modulates nociception is still unclear. Pharmacological studies have implicated the opening of calcium-operated potassium channels (*11*), but the existence of other mechanisms cannot be ruled out.

The present report shows that, in addition to participating in the control of nociception, NAAA-regulated PEA signaling at PPAR-α also governs the progression to pain chronicity by serving, at a critical juncture of the pain consolidation process, as a regulatory checkpoint for spinal cord metabolism. This hypothesis is consistent with the established roles of PPAR-α in the transcriptional control of lipid and glucose use (*12*) and is supported by three lines of evidence. First, formalin injection into the mouse hind paw causes a short-lived rise in NAAA expression in ipsilateral L4–L6 spinal cord, which reaches its maximum 72 hours after the injury (Fig. 7C). This coincides with a transcriptionally regulated switch in cellular bioenergy production from mitochondrial respiration to aerobic glycolysis and pentose phosphate metabolism (further discussed below). Second, systemic or intrathecal administration of one of three different NAAA inhibitors at the peak of NAAA expression (i.e., 48 to 72 hours after the injury) shuts off this metabolic switch and simultaneously stops the transition to CPLS (Fig. 7I and fig. S8, G to K). Third, mutant mice lacking *Naaa* do not progress to CPLS even when they are challenged with a suprathreshold dose of formalin

(3%) that evokes substantial nocifensive behavior, local inflammation, and ipsilateral hypersensitivity (Fig. 4, D to F, and fig. S4, C1 to C3). These disease-modifying properties of NAAA inhibitors can be readily distinguished from those of other therapeutic drug classes. We found that four analgesic and anti-inflammatory agents used in the clinic—morphine, gabapentin, ketamine, and ketoprofen—fail to prevent CPLS when administered at the peak of NAAA inhibitor efficacy. On the other hand, administration of an NAAA inhibitor during this critical period stops CPLS development but does not affect the size of the inflammatory response or the time course of its resolution. Furthermore, NAAA inhibitors do not visibly accelerate tissue healing, as seen, for example, with agents that block fatty acid amide hydrolase activity (*64*). To mark the ability of NAAA inhibitors and PPAR-α agonists to halt the progression to pain chronicity—which differentiates them from analgesic, anti-inflammatory, proresolving, and proreparative agents—we used the neologism "algostatic" from Ancient Greek ἄλγος (pain) and ἱστάναι (to stop).

The role of cellular energy metabolism in the transition to chronic pain after tissue injury deserves consideration. End-organ damage poses an extraordinary bioenergetic challenge to first- and second-order nociceptors, as it pressures them to enact large-scale neuroplastic adaptations while simultaneously maintaining energy homeostasis along the considerable distance of their axonal trees (>1 m in humans) (*65*). Finite neuronal resources must be allocated to two equally urgent tasks: heightened energy production to sustain the upsurge in neural activity caused by the lesion, and biomass generation to effect the structural changes needed to support peripheral and central sensitization (*16*). The results of our transcriptomic and metabolomic experiments suggest that mouse spinal cord neurons negotiate this conflict—most likely in concert with cells of other lineages (see further discussion below)—by temporarily shifting ATP production from mitochondrial respiration, which is energetically efficient but has substantial proteomic costs (*66*), to Warburg-like aerobic glycolysis (*17*), which is far less efficient but can generate carbon units for protein and lipid biosynthesis. A maladaptive consequence of this metabolic switch, whose occurrence in differentiating (*67*) and acutely stimulated adult neurons (*68*, *69*) is documented, is the instigation of an energy crisis that might disrupt electrochemical gradients and ultimately precipitate central sensitization. An interesting parallel of this hypothetical scenario is offered by macrophages, which shift their metabolism toward glycolysis when transitioning to trained immunity (*70*), a sensitized state that heightens both their responsiveness to recurring infections and the risk of unleashing a hyperinflammatory reaction (*71*). This phenotype shift is stopped by the antidiabetic drug metformin (*71*), which also prevents neuropathic pain in male (but not female) rodents (*72*). In both instances, metformin may work by indirectly recruiting AMP-activated protein kinase, which reacts to cellular energy crises by stimulating ATP generation and suppressing anabolic processes (*73*). Despite their obvious dissimilarities, these two responses to noxious signals appear to rely on a shared proteome allocation strategy that transiently favors aerobic glycolysis over oxidative phosphorylation—a suboptimal trade-off (*49*) that may render affected cells persistently hypersensitive to an otherwise innocuous stimulus.

The present results raise three important questions. The first pertains to the identity of the cellular elements involved in the algostatic effects of NAAA inhibition. Spinal cord neurons constitutively express NAAA and may be directly affected by NAAA blockade. But the enzyme (or the mRNA encoding for it) is also found in spinal astrocytes and microglia [(*74*), http://neuroexpresso.org] as well as in circulating monocytes and resident tissue macrophages (*9*), whose roles in the pathogenesis and resolution of chronic pain are well recognized (*75*, *76*). Our finding that NAAA overexpression in $CD11b^+$ cells (i.e., monocytes, macrophages, and microglia) facilitates the induction of CPLS (Fig. 4, J to L) suggests that at least one of these cell types may be targeted by NAAA inhibitors. The second question relates to the role that NAAA might play in the resilient phenotype exhibited by 20% of male (not female) mice that exhibit normal acute responses to formalin but fail to transition to CPLS (Fig. 1, B and C). In humans, resilience toward developing chronic pain is sexually dimorphic (women are on average less resilient) (*47*, *77*) and depends on multiple preexisting factors that include age, genetic makeup, and disease history (*2*). Untangling NAAA's role in this complex scenario is an important topic for future research. The last question pertains to the mechanism through which nerve injury increases NAAA expression in spinal cord neurons. Given the paucity of information regarding NAAA's transcriptional control (*10*), a variety of scenarios appear equally plausible. One intriguing possibility is that release of colony stimulating factor 1 (*78*) or other cytokines (e.g., CXCL1) (*79*) in the dorsal horn might directly or indirectly stimulate NAAA transcription. In this regard, it is important to point out that NAAA may also be activated through a posttranslational mechanism involving the autocatalyzed cleavage of its inactive precursor (*10*).

The above questions notwithstanding, the present results identify a previously unrecognized control node in the transition from acute to chronic pain, which can be targeted by NAAA inhibitors or by other agents that enhance PEA-mediated signaling at PPAR-α. Owing to their distinctive pharmacological profile—which combines antinociception, anti-inflammation, and algostasis—NAAA inhibitors might find clinical application in the treatment of various forms of chronic pain as well as in perioperative strategies aimed at preventing the establishment of central sensitization caused by incisional and inflammatory injuries (*80*).

MATERIALS AND METHODS

Chemicals

ARN19702, ARN16186, and ARN077 were synthesized following established procedures (*10*). For ARN16186, sodium borohydride reduction of tert-butyl 3-oxo-8-azabicyclo[3.2.1]octane-8-carboxylate gave an endo/exo mixture of the corresponding 3-hydroxy isomers that were separated by column chromatography. Etherification of the (exo)-3-hydroxy isomer with 4-butylphenol under Mitsunobu conditions, followed by N-Boc deprotection [trifluoroacetic acid/dichloromethane (TFA/DCM), 1:3], yielded the corresponding (endo)-3-(4-butylphenoxy)-8-azabicyclo[3.2.1]octane, which was then submitted to *N*-sulfonylation with 3,5-dimethyl-lH-pyrazole-4-sulfonyl chloride, in the presence of sodium hydride, to yield ARN16186. Formalin, capsaicin, morphine sulfate, gabapentin, ketamine hydrochloride (solution, 100 mg-ml^{-1}), ketoprofen, GW7647, GW6471, and fenofibrate were from Sigma-Aldrich (St. Louis, USA). A proprietary water-soluble PEA formulation (Levagen Plus) was manufactured at Shilpa Medicare Ltd. (Raichur, India) and was a gift of Gencor (Irvine, CA). [$^2H_4$]-PEA was from Cayman Chemicals (Ann Harbor, USA). All solvents and chemicals were of the highest available grade.

Animals

We used C57BL/6J mice (10 to 12 weeks old, 24 to 26 g; #000664) unless otherwise indicated. *Ppar*^{tnjGonz}-targeted mutation (*Ppara*$^{-/-}$; #008154) mice were purchased from the Jackson Laboratory (Bar Harbor, ME, USA). *Naaa*$^{-/-}$ mice [B6N-A^{tm1Brd}*Naaa*$^{tm1a(KOMP)wtsi}$/WtsiH] were acquired from MRC Harwell (Didcot, UK) through the EMMA-European Mouse Mutants Archive (*36*). This mouse line was generated as a knockout first, reporter-tagged insertion with conditional potential allele. *Naaa*$^{-/-}$ mice were obtained by mating animals heterozygous for the *Naaa*$^{tm1a(KOMP)wtsi}$ allele. NAAA deletion was confirmed by reverse transcription polymerase chain reaction (RT-PCR), Western blot, and enzyme activity measurements, as described (*81*). Mice overexpressing NAAA in CD11b^{+} monocyte-derived cells (*Naaa*$^{CD11b+}$) were generated as follows (*81*). Heterozygous NAAA conditional knock-in mice were produced at GenoWay (Lyon, France) by targeted insertion of the *Naaa* gene within the Rosa26 locus using GenoWay's Quick Knock-in technology. A loxP flanked transcriptional stop cassette was incorporated between the transgene and the synthetic CAGG promoter to allow the expression of the resulting transgene to be dependent on Cre recombinase. These "Rosa26 knock-in" mice were used to produce homozygous animals, which were then cross-bred with CD11b-Cre mice (the Jackson Laboratory) to generate the *Naaa*$^{CD11b+}$ line. The mice were maintained in a pathogen-free environment on 12-hour light/dark cycle at controlled temperature (22°C) and humidity (50 to 60%). Food and water were available ad libitum.

Animals were randomly assigned to treatment groups and, before the start of the experiments, were handled for three consecutive days (~3 min per animal/day), and behavioral testing was conducted during the light phase of the light/dark cycle. Efforts were made to minimize the number of animals used and their discomfort. The study complied with all ethical regulations of the National Institutes of Health (NIH) *Guide for the Care and Use of Laboratory Animals* and the recommendation of the International Association for the Study of Pain. Experimental procedures were approved by the Animal Care and Use Committee of the University of California, Irvine (AUP-20-117).

Drug administration

Drug solutions were prepared shortly before use. Capsaicin was dissolved in a vehicle of Tween 80 distilled water (7/93, vol), sonicated, and filtered before intraplantar injection. Gabapentin, morphine, and PEA were dissolved in distilled water. Gabapentin was administered by intraperitoneal injection, and morphine and PEA were administered by subcutaneous injection. Ketoprofen, ARN19702, ARN16186, ARN077, GW7647, GW6471, and fenofibrate were dissolved in polyethylene glycol 400/Tween 80/distilled water (15/15/70, vol) and administered by intraperitoneal or intrathecal injection. An appropriate volume of the commercial ketamine solution was administered by the intraperitoneal route. For intrathecal administration, the mice were anesthetized with isoflurane (3 to 5% in oxygen). Percutaneous injections were made at intervertebral space L5–L6 with a 30-gauge needle perpendicular to the skin. Injectate volumes of 5 μl were delivered using a 10-μl Hamilton syringe, and placement was confirmed by a lateral tail flick as the needle entered the subarachnoid space.

RNA isolation and quantitative RT-PCR

We extracted total RNA from lumbar spinal cord fragments (L4–L6) ipsilateral and contralateral to the formalin injection site using the TRIzol reagent (Thermo Fisher Scientific, Waltham, USA). RNA was purified with PureLink RNA Mini Kit (Invitrogen, Carlsbad, USA). Before purification, samples were rendered genomic DNA free by passing the isolated RNA through a gDNA Eliminator spin column (Qiagen, Germantown, USA). RNA concentration and purity were determined using a NanoDrop 2000/2000-c spectrophotometer (Thermo Fisher Scientific). cDNA was synthesized using 2 μg of total RNA as input for the High-Capacity cDNA RT Kit with RNase Inhibitor (Applied BioSystems, Foster City, USA) with a final reaction volume of 20 μl. First-strand cDNA was amplified using TaqMan Universal PCR Master Mix (Thermo Fisher Scientific) following the manufacturer's instructions. RT-PCR primers and fluorogenic probes were purchased from Applied Biosystems [TaqMan(R) Gene Expression Assays]. We used TaqMan gene expression assays for mouse actin-β (Mm00607939_s1), *Hprt* (Mm00446968_m1), *Gapdh* (Mm99999915_g1), and *Naaa* (Mm01341699_m1) (Applied Biosystems). RT-PCRs were performed in 96-well plates using CFX96 Real-Time System (Bio-Rad, Hercules, USA). The Bestkeeper software was used to determine the expression stability and the geometric mean of three different housekeeping genes (*Actb*, *Hprt*, and *Gapdh*). The relative quantity of genes of interest was calculated by the $2^{-\Delta\Delta Ct}$ method and expressed as fold change over vehicle controls.

Lipid extraction

Lumbar L4–L6 spinal cord fragments (~15 mg each) were transferred into 2-ml Precellys soft tissue tubes (Bertin Instruments, France) and diluted with ice-cold acetone (1 ml) containing [$^{2}H_{4}$]-PEA (50 μl, 100 nM). Samples were homogenized at 4°C, 6000 rpm, 15 s per cycle for two cycles with a 20-s pause in between cycles. Supernatants were transferred into 8-ml glass vials and dried under nitrogen. Chloroform/methanol (2/1, vol, 3 ml) and water (1 ml) were added to the samples, which were then stirred vigorously and centrifuged at 830*g* for 15 min at 4°C. The lower (organic) phases were collected, and upper phases were extracted again with chloroform (2 ml) and combined with the previous extract. Extracts were dried under nitrogen, reconstituted in acetonitrile (0.1 ml), transferred to deactivated glass inserts, and placed inside amber glass vials for liquid chromatography/tandem mass spectrometry analyses.

PEA quantification

PEA was fractionated using a 1260 series LC system (Agilent Technologies, Santa Clara, CA) coupled to a 6460C triple-quadrupole mass spectrometric detector (MSD; Agilent). A step gradient separation was performed on an Eclipse XDB C18 column (1.8 μm, 2.1 × 30.0, or 50.0 mm; Agilent) with a mobile phase consisting of water containing 0.25% acetic acid and 5 mM ammonium acetate as solvent A and methanol containing 0.25% acetic acid and 5 mM ammonium acetate as solvent B. The gradient conditions were as follows: starting at 78% B to 28% B in 8.00 min, changed to 95% B at 8.01 min, and maintained until 10.00 min; then changed back to 78% B at 10.01 min; the equilibration time was 5 min. The flow rate was 0.3 to 0.5 ml min^{-1}. The autosampler was maintained at 9°C, and the column at 40°C. Injection volume was 2 μl. To prevent carryover, the needle was washed three times in the autosampler port for 30 s before each injection using a wash solution consisting of 10% acetone in water/methanol/isopropanol/acetonitrile (1/1/1/1, vol). The MSD was operated in the positive electrospray ionization

mode, and analytes were quantified by multiple reaction monitoring. Capillary and nozzle voltages were 3500 and 300 to 500 V, respectively. Drying gas temperature was 300° to 350°C with a flow of 9.0 to11.0 liter/min. Sheath gas temperature was 300° to 375°C with a flow of 12 liter min^{-1}. Nebulizer pressure was set at 45 to 50 psi. We used the MassHunter software (Agilent) for instrument control, data acquisition, and analysis.

RNA sequencing and bioinformatics analysis

We extracted total RNA with the RNeasy Mini Kit (Qiagen). Samples with RNA integrity number ≥8.5 were kept for library construction. cDNA synthesis, amplification, library construction, and sequencing were performed at Novogene (Beijing, China) using the Illumina NovaSeq platform with paired-end 150–base pair sequencing strategy. Downstream analysis was performed using a combination of programs including STAR, HTseq, Cufflink. and Novogene's wrapped scripts. Alignments were parsed using the STAR program, and differential expressions were determined using DESeq2/edgeR. GO and Kyoto Encyclopedia of Genes and Genomes enrichment were implemented using the ClusterProfiler. GO terms with adjusted $P < 0.05$ were considered significantly enriched in differential expressed genes.

Metabolomic analysis

Metabolomics analyses were performed at the West Coast Metabolomics Center of the University of California Davis, as described (*82*). Briefly, frozen lumbar spinal cord (L4–L6) fragments (~5 mg) were homogenized in Eppendorf tubes (2 ml) for 2 min using metal spheres (20-mm diameter) in an MM300 mill (Retsch, Germany). A mixture of isopropanol/acetonitrile/water (3/3/2, vol) was added to the grounded tissue (1 ml per 20 mg), stirred for 10 s, and shaken at 4°C for 5 min. After centrifugation at 14,000*g* for 2 min, the supernatant was collected and concentrated to dryness in a CentriVap Cold Traps vacuum concentrator (Labconco, Kansas City, USA) at room temperature for 4 hours. Derivatization for gas chromatography time-of-flight mass spectrometry was carried out as described (*83*). Metabolites were identified based on retention time and spectral properties using the BinBase algorithm (https://fiehnlab.ucdavis.edu/projects/binbase-setup) and were matched against an internal mass spectral library. They were reported if present in at least 80% of the samples.

General histological procedures

Mice were anaesthetized with isoflurane, transcardially flushed with cold phosphate-buffered saline (PBS), and perfused with 4% paraformaldehyde (PFA) in PBS. Spinal cords were extruded, postfixed in PFA/PBS for 24 hours, and cryoprotected in sucrose (30% in PBS) at 4°C. Three to six series of transverse sections (40-µm thickness) were collected using a cryostat and stored at −20°C.

Confocal microscopy

Double and triple immunostaining experiments were performed by sequential incubation with primary antibodies [anti-NAAA (1:100; Invitrogen, Carlsbad, USA, PA5-69357), anti-NeuN (1:100; Cell Signaling Technology, Danvers, USA, clone E4M5P #94403), anti-GFAP (1:200; Abcam, Burlingame, USA, #Ab10062), anti-Olig2 (1:200; Millipore, Hayward, USA, #MABN50), and anti-CD11b (1:100; Bio-Rad, Irvine, USA, #MCA711G)] followed by appropriate secondary Alexa Fluor antibodies (1:1000; Invitrogen). Validation of the anti-NAAA antibody is provided in fig. S7 (A to D). Images were collected using an Olympus (Tokyo, Japan) FV3000 confocal microscope with a 10/40× 0.4/1.25 numerical aperture objective lens. Quantification of fluorescence intensity was performed using the NIH Fuji Is Just ImageJ (FIJI) software on a minimum of three images per animal.

Fos immunohistochemistry

Two weeks after formalin injection, the hind paw contralateral to the formalin injection site was challenged with capsaicin (0.1 µg, intraplantar). Two hours later, the mice were euthanized and perfused with ice-cold PBS and then with 4% PFA in PBS, and the lumbar spinal cord was removed and processed as described above. Free-floating sections (30 µm) were immersed in PBS containing hydrogen peroxide (0.3%), and nonspecific binding was removed by incubation (1 hour) with 5% goat serum and 0.3% Triton X-100 in 0.1 M PBS, followed by incubation (48 hour) at 4°C with a rabbit anti–c-Fos antibody (1:1000; Cell Signaling Technology, #2250). The tissue was incubated in the presence of biotinylated goat anti-rabbit immunoglobulin G followed by Vectastain Elite ABC reagent (1:600; Vector Laboratories, Burlingame, USA, #PK6101). Fos immunoreactivity was visualized with the avidin-biotin peroxidase method using diaminobenzidine as chromogen. Sections were washed with double-distilled water, slide mounted, air dried, dehydrated, and coverslipped with Permount. Slides were scanned using a Leica (Wetzlar, Germany) DM6B light microscope, and four to six sections per subject exhibiting the highest number of Fos-immunoreactive cells, based on qualitative evaluation, were imaged at ×10 magnification. Fos-expressing nuclei were counted using a computer-assisted image analysis system (LAS AF 2D, Leica) by an experimenter blinded to experimental conditions.

Behavioral tests

Formalin

We injected formalin (0.1, 0.3, 1, and 3% vol, 20 µl) or saline into the plantar surface of the right hind paw. Following injection, the mice were immediately transferred to a transparent observation chamber where nocifensive behavior (time spent licking or biting the injected paw and number of paw shakings) was videorecorded for 60 min and quantified by blinded observer. Mechanical allodynia, heat hyperalgesia, and paw edema were measured on PFD7, 14, 21, 60, and 120 in both injected and noninjected paws.

Capsaicin

Capsaicin or its vehicle was injected into the plantar surface of the left hind paw (20 µl) or left forepaw (10 µl), i.e., contralaterally to the formalin injection site. Nocifensive behavior was videorecorded for 10 min and evaluated under blinded conditions. Outcome measures after hind paw injection included the following: time spent licking or biting the injected paw and number of paw shaking episodes; outcome measures after forepaw injection also included number of paw rubbing episodes (movie S1).

Chronic constriction injury

CCI of the sciatic nerve was carried out as described (*37*). Briefly, the mice were anesthetized with isoflurane, and the right common sciatic nerve was exposed at the level of the middle thigh by blunt dissection under aseptic conditions. Proximal to the trifurcation, the nerve was cleaned from surrounding connective tissue, and three chromic cat gut ligatures (4-0, Ethicon, Somerville, USA) were loosely tied around it at 1-mm intervals. The wound was closed with a single muscle suture and skin clips. In sham-operated animals, the nerve was exposed but not tied.

Mechanical allodynia

Mechanical allodynia was assessed using a dynamic plantar aesthesiometer (Ugo Basile, Comerio, Italy). After a 45-min habituation period in transparent cages positioned on a wire mesh surface, a mechanical stimulus was applied to the plantar surface of both hind paws by an automated steel filament exerting an increasing force ranging from 0 to 5 g over 10 s. Three withdrawal thresholds (in grams) were recorded and averaged.

Paw edema

Paw edema was measured with a digital caliper (Fisher Scientific, USA) and is expressed as the difference (Δpaw thickness, mm) between ipsilateral and contralateral paws.

Sensitivity to heat

Sensitivity to heat was measured using a Hargreaves plantar test apparatus (San Diego Instruments, San Diego, USA). After a 45-min habituation period, the plantar surface of both hind paws was exposed to a beam of radiant heat through the glass floor. The cutoff time was set at 15 s. The stimulation was repeated three times with an interval of 2 min between stimuli, and latencies (in second) to withdraw the paw were recorded and averaged.

Elevated plus maze test

We placed each mouse in the central platform of the maze, facing the open arm opposite to the experimenter, and behavior was recorded using the Debut video capture software (NCH Software, Canberra, Australia). A blinded observer measured the amount of time spent in the open and closed arms, as well as the number of open and closed arm entries. The open arms of the maze were illuminated at 150 to 170 lux, and the closed arms at 40 to 50 lux. The anxiety index was calculated as follows

$$\text{Anxiety index} = 1 - \frac{\left(\frac{\text{time in open arms}}{\text{total time}}\right) + \left(\frac{\text{number of open arms entries}}{\text{total entries}}\right)}{2}$$

Novel object recognition test

Novel object recognition test was performed as described (*59*). The test was conducted over 3 days. On day 1, mice were habituated to the empty arena for 20 min. On day 2, they were returned to the arena, which now contained two identical objects. On day 3, one of the objects was replaced with another one of different shape, color, and texture. Mice were allowed to explore the arena for 10 min, and the total time spent exploring each object (i.e., nosing and sniffing at a distance ≤2 cm) was recorded by a blinded observer. The discriminatory index was calculated as follows

$$\text{Discriminatory index} = \frac{(\text{time of novel object exploration}) - (\text{time of familiar object exploration})}{\text{total exploration time}}$$

Feeding and motor activity

We habituated animals to the test cages for 3 days before trials. Food intake and motor activity were recorded for 24 hours using an automated system (TSE, Bad Homburg, Germany). The system, protocol, and feeding parameters surveyed were previously described (*84*). Motor activity was recorded using an *X*-*Y* matrix of infrared sensors and is reported as number of beam breaks in 24 hours.

Conditioned placed preference

To determine whether end-organ damage resulted in long-lasting ongoing or spontaneous pain (*85*), mice were subjected to either formalin (1%) injection or CCI injury as described above, and a single-trial CPP test was performed 14 days later. The test consisted of three phases: preconditioning, conditioning, and preference assessment.

Preconditioning

Twelve days after tissue damage, mice were placed in the two-chamber CPP apparatus [for details, see (*63*)], and the time spent in each chamber was recorded for 10 min and analyzed to determine preconditioning baseline. Individual mice that showed more than 80% of preference during preconditioning were excluded.

Conditioning

Mice underwent single-trial conditioning 24 hours after preconditioning using a biased approach. In the morning of the conditioning day, animals received saline and were immediately placed into the preferred chamber (saline paired) of the CPP box for 30 min with no access to the other chambers. Approximately 4 hours later, mice received gabapentin (50 mg kg^{-1}, IP) and were immediately confined in the nonpreferred chamber for 30 min (gabapentin paired).

Preference test

On the test day (POD14 or PFD14), 12 hours after the afternoon pairing, mice were placed back into the center of the CPP chambers with free access to all chambers for 10 min. Time (s) spent in each chamber was recorded and evaluated by a blind observer to determine preference.

Magnetic resonance imaging acquisition

Mice were anesthetized, flushed intracardially with ice-cold PBS and then with 4% PFA in PBS (pH 7.4). Brains and spinal cords were removed within their osseous structures and postfixed overnight in 4% PFA, followed by three 5-min washes with PBS the next day, and stored in PBS (pH 7.4) containing sodium azide (0.02%, weight) at 4°C. Ex vivo DTI and T2-weighted imaging (T2WI) studies were performed using a 9.4T Bruker Avance imager (Bruker Biospin, Billerica, USA). Data were acquired with the following parameters: 1.5-cm field of view, 0.5-mm slice thickness, and a 128 × 128 acquisition matrix and zero filled to 256 × 256. DTI parameters were as follows: repetition time (TR)/echo time (TE) = 8000 ms/35.66 ms, 30 isolinear directions, B = 3000 mT/m, and five B0 images acquired before weighted images. T2WI parameters were TR/TE = 4000/10 ms with 10 equally spaced echoes.

Magnetic resonance imaging acquisition processing and analyses

Brain

We used three-dimensional (3D) automatic registration for unbiased region parcellation to analyze DTI metrics in brain structures. Scans underwent eddy current correction, and brain was digitally removed from surrounding skull and muscles using 3D Pulse-Coupled Neural Networks (PCNN3D v1.2) in MATLAB R2017a (MathWorks). Extraction masks were reviewed and adjusted by a blinded experimenter using ITK Snap (version 3.8.0). T2 maps were generated using FMRIB's Software Library (FSL v5.0; FMRIB, Oxford, UK). FMRIB's Diffusion Toolbox was used to generate parametric DTI maps, in which a diffusion tensor model was fit at each voxel (*86*). The Australian Mouse Brain Atlas Consortium atlas (*87*) was fit to each individual animal, and regional labels were

applied with Advanced Normalization Tools. Regional statistics for T2 values, FA, mean diffusivity (MD), axial diffusivity (AD), and radial diffusivity (RD) were extracted for 80 bilateral regions. Regional volumes were extracted from T2 scans. This robust method allows an unbiased and rapid segmentation of GM and white matter (WM) regions from the mouse brain.

Spinal cord

Magnetic resonance imaging scans were processed for eddy current correction as outlined above, and the scans were manually masked and extracted using ITK Snap (version 3.8.0). Masks were reviewed and adjusted by a blinded experimenter. FMRIB's Diffusion Toolbox was used to generate parametric DTI maps. The resultant maps were then analyzed in DSI studio (http://dsi-studio.labsolver.org). Distinct regions of interest throughout the spinal cord were drawn manually [see (*63*) for accurate identification of spinal cord segments] for each animal without right/left distinction for WM and GM. Regional average value of the diffusion indices (FA, MD, AD, and RD) and volume were automatically extracted for each spinal cord segments.

Statistical analyses

Data are presented as means ± SEM. Statistical significance was determined using unpaired two-tailed Student's *t* test (with or without Bonferroni's correction) or analysis of variance (ANOVA) (one way, two way, and multifactorial) followed by Dunnett's or Bonferroni's post hoc test, as appropriate. Analyses were performed with either GraphPad Prism version 8.0 (GraphPad Prism) or the Statistical Package for Social Science program SPSS (SPSS). The D'Agostino-Pearson normality test was used to determine the distribution of the population of formalin-injected mice (Fig. 1 and figs. S1, C to E, and S2, G and H). A k-means cluster analysis with 10 iterations followed by one-way ANOVA separated two groups of mice, which were termed "resilient" and "vulnerable" based on their enduring response to formalin. Data analyses were performed under blinded conditions, and sample size was not predetermined.

SUPPPLEMENTARY MATERIALS

Supplementary material for this article is available at https://science.org/doi/10.1126/sciadv.abi8834

View/request a protocol for this paper from *Bio-protocol*.

REFERENCES AND NOTES

1. C. R. Chapman, C. J. Vierck, The transition of acute postoperative pain to chronic pain: An integrative overview of research on mechanisms. *J. Pain* **18**, 359.1–359.e38 (2017).
2. F. Denk, S. B. McMahon, I. Tracey, Pain vulnerability: A neurobiological perspective. *Nat. Neurosci.* **17**, 192–200 (2014).
3. A. I. Basbaum, D. M. Bautista, G. Scherrer, D. Julius, Cellular and molecular mechanisms of pain. *Cell* **139**, 267–284 (2009).
4. R. R. Ji, A. Chamessian, Y. Q. Zhang, Pain regulation by non-neuronal cells and inflammation. *Science* **354**, 572–577 (2016).
5. T. J. Price, A. I. Basbaum, J. Bresnahan, J. F. Chambers, Y. De Koninck, R. R. Edwards, R. R. Ji, J. Katz, A. Kavelaars, J. D. Levine, L. Porter, N. Schechter, K. A. Sluka, G. W. Terman, T. D. Wager, T. L. Yaksh, R. H. Dworkin, Transition to chronic pain: Opportunities for novel therapeutics. *Nat. Rev. Neurosci.* **19**, 383–384 (2018).
6. F. Marchand, M. Perretti, S. B. McMahon, Role of the immune system in chronic pain. *Nat. Rev. Neurosci.* **6**, 521–532 (2005).
7. E. K. Joseph, J. D. Levine, Mitochondrial electron transport in models of neuropathic and inflammatory pain. *Pain* **121**, 105–114 (2006).
8. G. J. Bennett, T. Doyle, D. Salvemini, Mitotoxicity in distal symmetrical sensory peripheral neuropathies. *Nat. Rev. Neurol.* **10**, 326–336 (2014).
9. K. Tsuboi, L. Y. Zhao, Y. Okamoto, N. Araki, M. Ueno, H. Sakamoto, N. Ueda, Predominant expression of lysosomal N-acylethanolamine-hydrolyzing acid amidase in macrophages revealed by immunochemical studies. *Biochim. Biophys. Acta* **1771**, 623–632 (2007).
10. D. Piomelli, L. Scalvini, Y. Fotio, A. Lodola, G. Spadoni, G. Tarzia, M. Mor, N-Acylethanolamine Acid Amidase (NAAA): Structure, function, and inhibition. *J. Med. Chem.* **63**, 7475–7490 (2020).
11. J. LoVerme, R. Russo, G. La Rana, J. Fu, J. Farthing, G. Mattace-Raso, R. Meli, A. Hohmann, A. Calignano, D. Piomelli, Rapid broad-spectrum analgesia through activation of peroxisome proliferator-activated Receptor-α. *J. Pharmacol. Exp. Ther.* **319**, 1051–1061 (2006).
12. N. Bougarne, B. Weyers, S. J. Desmet, J. Deckers, D. W. Ray, B. Staels, K. De Bosscher, Molecular Actions of PPARα in Lipid Metabolism and Inflammation. *Endocr. Rev.* **39**, 760–802 (2018).
13. B. B. Artukoglu, C. Beyer, A. Zuloff-Shani, E. Brener, M. H. Bloch, Efficacy of palmitoylethanolamide for pain: A meta-analysis. *Pain Physician* **20**, 353–362 (2017).
14. L. Rankin, C. J. Fowler, The basal pharmacology of palmitoylethanolamide. *Int. J. Mol. Sci.* **21**, 7942 (2020).
15. C. Annunziata, A. Lama, C. Pirozzi, G. Cavaliere, G. Trinchese, F. Di Guida, A. Nitrato Izzo, F. Cimmino, O. Paciello, D. De Biase, E. Murru, S. Banni, A. Calignano, M. P. Mollica, G. Mattace Raso, R. Meli, Palmitoylethanolamide counteracts hepatic metabolic inflexibility modulating mitochondrial function and efficiency in diet-induced obese mice. *FASEB J.* **34**, 350–364 (2020).
16. A. Latremoliere, C. J. Woolf, Central sensitization: A generator of pain hypersensitivity by central neural plasticity. *J. Pain* **10**, 895–926 (2009).
17. M. V. Liberti, J. W. Locasale, The warburg effect: How does it benefit cancer cells? *Trends Biochem. Sci.* **41**, 211–218 (2016).
18. D. Dubuisson, S. G. Dennis, The formalin test: A quantitative study of the analgesic effects of morphine, meperidine, and brain stem stimulation in rats and cats. *Pain* **4**, 161–174 (1977).
19. L. Luongo, F. Guida, S. Boccella, G. Bellini, L. Gatta, F. Rossi, V. de Novellis, S. Maione, Palmitoylethanolamide reduces formalin-induced neuropathic-like behaviour through spinal glial/microglial phenotypical changes in mice. *CNS Neurol. Disord. Drug Targets* **12**, 45–54 (2013).
20. K. Y. Fu, A. R. Light, G. K. Matsushima, W. Maixner, Microglial reactions after subcutaneous formalin injection into the rat hind paw. *Brain Res.* **825**, 59–67 (1999).
21. L. Arendt-Nielsen, Central sensitization in humans: Assessment and pharmacology. *Handb. Exp. Pharmacol.* **227**, 79–102 (2015).
22. K. H. Konopka, M. Harbers, A. Houghton, R. Kortekaas, A. van Vliet, W. Timmerman, J. A. den Boer, M. M. R. F. Struys, M. van Wijhe, Bilateral sensory abnormalities in patients with unilateral neuropathic pain; a quantitative sensory testing (QST) study. *PLOS ONE* **7**, e37524 (2012).
23. G. J. Asmundson, J. Katz, Understanding the co-occurrence of anxiety disorders and chronic pain: State-of-the-art. *Depress. Anxiety* **26**, 888–901 (2009).
24. K. S. Baker, S. Gibson, N. Georgiou-Karistianis, R. M. Roth, M. J. Giummarra, Everyday executive functioning in chronic pain: Specific deficits in working memory and emotion control, predicted by mood, medications, and pain interference. *Clin. J. Pain* **32**, 673–680 (2016).
25. A. E. Metz, H. J. Yau, M. V. Centeno, A. V. Apkarian, M. Martina, Morphological and functional reorganization of rat medial prefrontal cortex in neuropathic pain. *Proc. Natl. Acad. Sci. U.S.A.* **106**, 2423–2428 (2009).
26. M. N. Baliki, A. V. Apkarian, Nociception, pain, negative moods, and behavior selection. *Neuron* **87**, 474–491 (2015).
27. M. Kaushal, S. Shabani, M. Budde, S. Kurpad, Diffusion tensor imaging in acute spinal cord injury: A review of animal and human studies. *J. Neurotrauma* **36**, 2279–2286 (2019).
28. A. A. Schlegel, J. J. Rudelson, P. U. Tse, White matter structure changes as adults learn a second language. *J. Cogn. Neurosci.* **24**, 1664–1670 (2012).
29. S. Shiers, G. Pradhan, J. Mwirigi, G. Mejia, A. Ahmad, S. Kroener, T. Price, Neuropathic pain creates an enduring prefrontal cortex dysfunction corrected by the type II diabetic drug metformin but not by gabapentin. *J. Neurosci.* **38**, 7337–7350 (2018).
30. H. Eichenbaum, Prefrontal-hippocampal interactions in episodic memory. *Nat. Rev. Neurosci.* **18**, 547–558 (2017).
31. L. B. Haberly, Parallel-distributed processing in olfactory cortex: New insights from morphological and physiological analysis of neuronal circuitry. *Chem. Senses* **26**, 551–576 (2001).
32. N. Kataoka, Y. Shima, K. Nakajima, K. Nakamura, A central master driver of psychosocial stress responses in the rat. *Science* **367**, 1105–1112 (2020).
33. M. L. Lehmann, M. Herkenham, Environmental enrichment confers stress resiliency to social defeat through an infralimbic cortex-dependent neuroanatomical pathway. *J. Neurosci.* **31**, 6159–6173 (2011).
34. F. L. Hitti, S. A. Siegelbaum, The hippocampal CA2 region is essential for social memory. *Nature* **508**, 88–92 (2014).
35. G. Ji, V. Neugebauer, Hemispheric lateralization of pain processing by amygdala neurons. *J. Neurophysiol.* **102**, 2253–2264 (2009).
36. O. Sasso, M. Summa, A. Armirotti, S. Pontis, C. De Mei, D. Piomelli, The N-Acylethanolamine acid amidase inhibitor ARN077 suppresses inflammation

and pruritus in a mouse model of allergic dermatitis. *J. Invest. Dermatol.* **138**, 562–569 (2018).
37. G. J. Bennett, Y. K. Xie, A peripheral mononeuropathy in rat that produces disorders of pain sensation like those seen in man. *Pain* **33**, 87–107 (1988).
38. A. Nohturfft, S. C. Zhang, Coordination of lipid metabolism in membrane biogenesis. *Annu. Rev. Cell Dev. Biol.* **25**, 539–566 (2009).
39. C. J. Stefan, W. S. Trimble, S. Grinstein, G. Drin, K. Reinisch, P. De Camilli, S. Cohen, A. M. Valm, J. Lippincott-Schwartz, T. P. Levine, D. B. Iaea, F. R. Maxfield, C. E. Futter, E. R. Eden, D. Judith, A. R. van Vliet, P. Agostinis, S. A. Tooze, A. Sugiura, H. M. McBride, Membrane dynamics and organelle biogenesis-lipid pipelines and vesicular carriers. *BMC Biol.* **15**, 102 (2017).
40. D. Gomez-Varela, A. M. Barry, M. Schmidt, Proteome-based systems biology in chronic pain. *J. Proteome* **190**, 1–11 (2019).
41. M. Yi, Y. Ban, Y. Tan, W. Xiong, G. Li, B. Xiang, 6-Phosphofructo-2-kinase/fructose-2,6-biphosphatase 3 and 4: A pair of valves for fine-tuning of glucose metabolism in human cancer. *Mol. Metab.* **20**, 1–13 (2019).
42. J. B. Clark, N-acetyl aspartate: A marker for neuronal loss or mitochondrial dysfunction. *Dev. Neurosci.* **20**, 271–276 (1998).
43. J. B. Spinelli, H. Yoon, A. E. Ringel, S. Jeanfavre, C. B. Clish, M. C. Haigis, Metabolic recycling of ammonia via glutamate dehydrogenase supports breast cancer biomass. *Science* **358**, 941–946 (2017).
44. C. R. Hancock, J. J. Brault, R. L. Terjung, Protecting the cellular energy state during contractions: Role of AMP deaminase. *J. Physiol. Pharmacol.* **57** (Suppl. 10), 17–29 (2006).
45. A. Warden, J. Truitt, M. Merriman, O. Ponomareva, K. Jameson, L. B. Ferguson, R. D. Mayfield, R. A. Harris, Localization of PPAR isotypes in the adult mouse and human brain. *Sci. Rep.* **6**, 27618 (2016).
46. D. S. Goldberg, S. J. McGee, Pain as a global public health priority. *BMC Public Health* **11**, 770 (2011).
47. J. Dahlhamer, J. Lucas, C. Zelaya, R. Nahin, S. Mackey, L. DeBar, R. Kerns, M. Von Korff, L. Porter, C. Helmick, Prevalence of chronic pain and high-impact chronic pain among adults - United States, 2016. *MMWR Morb. Mortal. Wkly Rep.* **67**, 1001–1006 (2018).
48. H. Reinecke, C. Weber, K. Lange, M. Simon, C. Stein, H. Sorgatz, Analgesic efficacy of opioids in chronic pain: Recent meta-analyses. *Br. J. Pharmacol.* **172**, 324–333 (2015).
49. B. Han, W. M. Compton, C. Blanco, E. Crane, J. Lee, C. M. Jones, Prescription opioid use, misuse, and use disorders in U.S. adults: 2015 national survey on drug use and health. *Ann. Intern. Med.* **167**, 293–301 (2017).
50. J. H. Rosland, A. Tjolsen, B. Maehle, K. Hole, The formalin test in mice: Effect of formalin concentration. *Pain* **42**, 235–242 (1990).
51. C. P. van Wilgen, K. H. Konopka, D. Keizer, J. Zwerver, R. Dekker, Do patients with chronic patellar tendinopathy have an altered somatosensory profile? A Quantitative Sensory Testing (QST) study. *Scand. J. Med. Sci. Sports* **23**, 149–155 (2013).
52. M. J. Bair, R. L. Robinson, W. Katon, K. Kroenke, Depression and pain comorbidity: A literature review. *Arch. Intern. Med.* **163**, 2433–2445 (2003).
53. G. M. Grace, W. R. Nielson, M. Hopkins, M. A. Berg, Concentration and memory deficits in patients with fibromyalgia syndrome. *J. Clin. Exp. Neuropsychol.* **21**, 477–487 (1999).
54. L. Goncalves, R. Silva, F. Pinto-Ribeiro, J. M. Pego, J. M. Bessa, A. Pertovaara, N. Sousa, A. Almeida, Neuropathic pain is associated with depressive behaviour and induces neuroplasticity in the amygdala of the rat. *Exp. Neurol.* **213**, 48–56 (2008).
55. M. G. Liu, J. Chen, Preclinical research on pain comorbidity with affective disorders and cognitive deficits: Challenges and perspectives. *Prog. Neurobiol.* **116**, 13–32 (2014).
56. R. D. Treede, W. Rief, A. Barke, Q. Aziz, M. I. Bennett, R. Benoliel, M. Cohen, S. Evers, N. B. Finnerup, M. B. First, M. A. Giamberardino, S. Kaasa, B. Korwisi, E. Kosek, P. Lavand'homme, M. Nicholas, S. Perrot, J. Scholz, S. Schug, B. H. Smith, P. Svensson, J. W. S. Vlaeyen, S. J. Wang, Chronic pain as a symptom or a disease: The IASP classification of chronic pain for the international classification of diseases (ICD-11). *Pain* **160**, 19–27 (2019).
57. N. Soliman, S. Haroutounian, A. G. Hohmann, E. Krane, J. Liao, M. Macleod, D. Segelcke, C. Sena, J. Thomas, J. Vollert, K. Wever, H. Alaverdyan, A. Barakat, T. Barthlow, A. L. H. Bozer, A. Davidson, M. Diaz-delCastillo, A. Dolgorukova, M. I. Ferdousi, C. Healy, S. Hong, M. Hopkins, A. James, H. B. Leake, N. M. Malewicz, M. Mansfield, A. K. Mardon, D. Mattimoe, D. P. McLoone, G. Noes-Holt, E. M. Pogatzki-Zahn, E. Power, B. Pradier, E. Romanos-Sirakis, A. Segelcke, R. Vinagre, J. A. Yanes, J. Zhang, X. Y. Zhang, D. P. Finn, A. S. C. Rice, Systematic review and meta-analysis of cannabinoids, cannabis-based medicines, and endocannabinoid system modulators tested for antinociceptive effects in animal models of injury-related or pathological persistent pain. *Pain* **162**, S26–S44 (2021).
58. D. Piomelli, O. Sasso, Peripheral gating of pain signals by endogenous lipid mediators. *Nat. Neurosci.* **17**, 164–174 (2014).
59. S. Pontis, A. Ribeiro, O. Sasso, D. Piomelli, Macrophage-derived lipid agonists of PPAR-αas intrinsic controllers of inflammation. *Crit. Rev. Biochem. Mol. Biol.* **51**, 7–14 (2016).
60. C. Solorzano, C. Zhu, N. Battista, G. Astarita, A. Lodola, S. Rivara, M. Mor, R. Russo, M. Maccarrone, F. Antonietti, A. Duranti, A. Tontini, S. Cuzzocrea, G. Tarzia, D. Piomelli, Selective N-acylethanolamine-hydrolyzing acid amidase inhibition reveals a key role for endogenous palmitoylethanolamide in inflammation. *Proc. Natl. Acad. Sci. U.S.A.* **106**, 20966–20971 (2009).
61. O. Sasso, G. Moreno-Sanz, C. Martucci, N. Realini, M. Dionisi, L. Mengatto, A. Duranti, G. Tarozzo, G. Tarzia, M. Mor, R. Bertorelli, A. Reggiani, D. Piomelli, Antinociceptive effects of the N-acylethanolamine acid amidase inhibitor ARN077 in rodent pain models. *Pain* **154**, 350–360 (2013).
62. I. A. Khasabova, Y. Xiong, L. G. Coicou, D. Piomelli, V. Seybold, Peroxisome proliferator-activated receptor α mediates acute effects of palmitoylethanolamide on sensory neurons. *J. Neurosci.* **32**, 12735–12743 (2012).
63. Y. Fotio, O. Sasso, R. Ciccocioppo, D. Piomelli, Antinociceptive profile of ARN19702, (2-Ethylsulfonylphenyl)-[(2S)-4-(6-fluoro-1,3-benzothiazol-2-yl)-2-methylpiperazin-1-yl] methanone, a novel orally ActiveN-Acylethanolamine acid amidase inhibitor, in animal models. *J. Pharmacol. Exp. Ther.* **378**, 70–76 (2021).
64. O. Sasso, S. Pontis, A. Armirotti, G. Cardinali, D. Kovacs, M. Migliore, M. Summa, G. Moreno-Sanz, M. Picardo, D. Piomelli, Endogenous N-acyl taurines regulate skin wound healing. *Proc. Natl. Acad. Sci. U.S.A.* **113**, E4397–E4406 (2016).
65. T. Misgeld, T. L. Schwarz, Mitostasis in neurons: Maintaining mitochondria in an extended cellular architecture. *Neuron* **96**, 651–666 (2017).
66. M. Basan, S. Hui, H. Okano, Z. Zhang, Y. Shen, J. R. Williamson, T. Hwa, Overflow metabolism in Escherichia coli results from efficient proteome allocation. *Nature* **528**, 99–104 (2015).
67. X. Zheng, L. Boyer, M. Jin, J. Mertens, Y. Kim, L. Ma, L. Ma, M. Hamm, F. H. Gage, T. Hunter, Metabolic reprogramming during neuronal differentiation from aerobic glycolysis to neuronal oxidative phosphorylation. *eLife* **5**, e13374 (2016).
68. G. Yellen, Fueling thought: Management of glycolysis and oxidative phosphorylation in neuronal metabolism. *J. Cell Biol.* **217**, 2235–2246 (2018).
69. C. Bas-Orth, Y. W. Tan, D. Lau, H. Bading, Synaptic activity drives a genomic program that promotes a neuronal Warburg effect. *J. Biol. Chem.* **292**, 5183–5194 (2017).
70. S.-C. Cheng, J. Quintin, R. A. Cramer, K. M. Shepardson, S. Saeed, V. Kumar, E. J. Giamarellos-Bourboulis, J. H. Martens, N. A. Rao, A. Aghajanirefah, G. R. Manjeri, Y. Li, D. C. Ifrim, R. J. Arts, B. M. van der Veer, P. M. Deen, C. Logie, L. A. O'Neill, P. Willems, F. L. van de Veerdonk, J. W. van der Meer, A. Ng, L. A. Joosten, C. Wijmenga, H. G. Stunnenberg, R. J. Xavier, M. G. Netea, mTOR- and HIF-1α-mediated aerobic glycolysis as metabolic basis for trained immunity. *Science* **345**, 1250684 (2014).
71. M. G. Netea, L. A. Joosten, E. Latz, K. H. Mills, G. Natoli, H. G. Stunnenberg, L. A. O'Neill, R. J. Xavier, Trained immunity: A program of innate immune memory in health and disease. *Science* **352**, aaf1098 (2016).
72. K. E. Inyang, T. Szabo-Pardi, E. Wentworth, T. A. McDougal, G. Dussor, M. D. Burton, T. J. Price, The antidiabetic drug metformin prevents and reverses neuropathic pain and spinal cord microglial activation in male but not female mice. *Pharmacol. Res.* **139**, 1–16 (2019).
73. D. G. Hardie, AMPK: A key regulator of energy balance in the single cell and the whole organism. *Int. J. Obes.* **32** (Suppl. 4), S7–S12 (2008).
74. B. O. Mancarci, L. Toker, S. J. Tripathy, B. Li, B. Rocco, E. Sibille, P. Pavlidis, Cross-laboratory analysis of brain cell type transcriptomes with applications to interpretation of bulk tissue data. *eNeuro* **4**, ENEURO.0212–ENEURO17.2017 (2017).
75. R. R. Ji, C. R. Donnelly, M. Nedergaard, Astrocytes in chronic pain and itch. *Nat. Rev. Neurosci.* **20**, 667–685 (2019).
76. K. Inoue, M. Tsuda, Microglia in neuropathic pain: Cellular and molecular mechanisms and therapeutic potential. *Nat. Rev. Neurosci.* **19**, 138–152 (2018).
77. M. L. Reitsma, J. E. Tranmer, D. M. Buchanan, E. G. Vandenkerkhof, The prevalence of chronic pain and pain-related interference in the Canadian population from 1994 to 2008. *Chronic Dis. Inj. Can.* **31**, 157–164 (2011).
78. X. Yu, A. Basbaum, Z. Guan, Contribution of colony-stimulating factor 1 to neuropathic pain. *Pain Rep.* **6**, e883 (2021).
79. X. Li, Q. Guo, Z. Ye, E. Wang, W. Zou, Z. Sun, Z. He, T. Zhong, Y. Weng, Y. Pan, PPAR γ prevents neuropathic pain by down-regulating CX3CR1 and attenuating M1 activation of microglia in the spinal cord of rats using a sciatic chronic constriction injury model. *Front. Neurosci.* **15**, 620525 (2021).
80. C. J. Woolf, M. S. Chong, Preemptive analgesia--treating postoperative pain by preventing the establishment of central sensitization. *Anesth. Analg.* **77**, 362–379 (1993).
81. S. Pontis, F. Palese, M. Summa, N. Realini, M. Lanfranco, C. De Mei, D. Piomelli, *N*-Acylethanolamine acid amidase contributes to disease progression in a mouse model of multiple sclerosis. *Pharmacol. Res.* **160**, 105064 (2020).
82. O. Fiehn, G. Wohlgemuth, M. Scholz, T. Kind, D. Y. Lee, Y. Lu, S. Moon, B. Nikolau, Quality control for plant metabolomics: Reporting MSI-compliant studies. *Plant J.* **53**, 691–704 (2008).
83. T. Kind, G. Wohlgemuth, D. Y. Lee, Y. Lu, M. Palazoglu, S. Shahbaz, O. Fiehn, FiehnLib: Mass spectral and retention index libraries for metabolomics based on quadrupole and time-of-flight gas chromatography/mass spectrometry. *Anal. Chem.* **81**, 10038–10048 (2009).

84. S. Gaetani, F. Oveisi, D. Piomelli, Modulation of meal pattern in the rat by the anorexic lipid mediator oleoylethanolamide. *Neuropsychopharmacology* **28**, 1311–1316 (2003).
85. E. Navratilova, J. Y. Xie, T. King, F. Porreca, Evaluation of reward from pain relief. *Ann. N. Y. Acad. Sci.* **1282**, 1–11 (2013).
86. J. L. R. Andersson, S. N. Sotiropoulos, An integrated approach to correction for off-resonance effects and subject movement in diffusion MR imaging. *NeuroImage* **125**, 1063–1078 (2016).
87. K. Richards, C. Watson, R. F. Buckley, N. D. Kurniawan, Z. Yang, M. D. Keller, R. Beare, P. F. Bartlett, G. F. Egan, G. J. Galloway, G. Paxinos, S. Petrou, D. C. Reutens, Segmentation of the mouse hippocampal formation in magnetic resonance images. *NeuroImage* **58**, 732–740 (2011).

Acknowledgments: We thank O. Sasso for invaluable help at the start of this project and A. Touwaide, C. M. Gall, G. Astarita, and O. Fiehn for discussion. **Funding:** NIH grant R41NS106999 (to D.P.), NIH grant R42DA033683 (to D.P.), and NIH grant DA041229 (to A.G.H.)
Author contributions: Conceptualization: Y.F. and D.P. Design: Y.F., A.G.H., A.O., and D.P. Investigation: Y.F., A.M.T., T.I.R., F.P., J.R., R.P., A.G.H., L.L., G.S., and M.M. Data analysis: Y.F., F.P., A.M.T., R.P., A.J., K.-M.J., A.O., A.G.H., and L.L. Funding acquisition: D.P. Project administration: D.P. Supervision: D.P. Writing, original draft: D.P. and Y.F. Writing, review and editing: D.P., Y.F., C.J., A.O., K.-M.J., A.G.H., and G.S. **Competing interests:** D.P. and M.M. are inventors in patents that protect ARN19702 and other NAAA inhibitors, owned by the University of California, the University of Parma, the University of Urbino, and the Fondazione Istituto Italiano di Tecnologia (no. 13/898,225, filed 20 May 2013, published 3 April 2014; no. 62/337,744, filed 17 May 2016, published 23 November 2017). D.P. and Y.F. are inventors in provisional patent application related to this work filed by the University of California (no. 63/166,134, filed 25 March 2021). The other authors declare that they have no competing interests. **Data and materials availability:** All data needed to evaluate the conclusions in the paper are present in the paper and/or the Supplementary Materials. Additional datasets (data S1 to S11) are available at https://doi.org/10.6084/m9.figshare.14903205.v1.

Submitted 6 April 2021
Accepted 1 September 2021
Published 22 October 2021
10.1126/sciadv.abi8834

Citation: Y. Fotio, K.-M. Jung, F. Palese, A. Obenaus, A. Mabou Tagne, L. Lin, T. I. Rashid, R. Pacheco, A. Jullienne, J. Ramirez, M. Mor, G. Spadoni, C. Jang, A. G. Hohmann, D. Piomelli, NAAA-regulated lipid signaling governs the transition from acute to chronic pain. *Sci. Adv.* **7**, eabi8834 (2021).